Molecular Physics
Vol. XX, No. XX, Month X 2013, 1–31

RESEARCH ARTICLE

Vibrational Tuning of the Hydrogen Transfer in Malonaldehyde – A combined FTIR and Raman Jet Study

Nils O. B. Lüttschwager,[a] Tobias N. Wassermann,[a,b] Stéphane Coussan,[b] and Martin A. Suhm[a,*]

[a] *Georg-August-Universität Göttingen, Institut für Physikalische Chemie, Tammannstr. 6, D-37077 Göttingen, Germany;* [b] *Laboratoire PIIM, Université de Provence, Centre Saint-Jérôme, Marseille F-13 397, cedex 20, France*

(*Submitted to Molecular Physics [special issue dedicated to Martin Quack]*)

Tunneling splittings in vibrationally excited malonaldehyde are derived from complementary FTIR and Raman spectra utilizing jet cooling and matrix isolation. Values from 0 to 69 cm^{-1} (*i. e.* from complete quenching of the proton tunneling to an acceleration by a factor of 3) are firmly assigned, underscoring a strong coupling between hydrogen transfer and vibrational excitation. More tentative assignments involve even larger effects for the O···O breathing vibration. The results are discussed with respect to the corresponding normal modes and compared to previous theoretical predictions.

Keywords: proton transfer; infrared spectroscopy; Raman scattering; vibrational dynamics; tunneling splittings

1. Introduction

The small mass of hydrogen leads to pronounced quantum delocalization even in the vibrational ground state of a molecule. If there is a symmetric double-minimum potential with a sufficiently low barrier along a hydrogen displacement coordinate, this gives rise to pronounced tunneling splittings of the vibrational energy levels. Famous examples are the $–NH_2$ group inversion in aniline [1], –OH torsion in H_2O_2 or phenol [2] and the hydrogen bond switching in the dimer of hydrogen fluoride [3]. In none of these cases, chemical bonds are broken along the path, unless one classifies a hydrogen bond as largely chemical in nature. The most prominent example which does involve a switch in chemical bonds is malonaldehyde (malondialdehyde, propanedial) in its enolic form [4, 5] (Figure 1). The O–H hydrogen is chemically bonded to one oxygen and hydrogen-bonded to the other. These two interactions can be interchanged upon a simultaneous rearrangement of single and double bonds in the six-membered chelating ring via a C_{2v} transition state (Figure 2). The resulting malonaldehyde tunneling splitting $\Delta\tilde{\nu}^0 \approx 21.6$ cm^{-1} [5] is comparable in size to the examples mentioned before, due to the short path and the resonance-assisted nature of the bond switching [6].

[Fig. 1 and Fig. 2 close to here]

The prototype character of malonaldehyde with its planar double minimum structure [7], narrow barrier [8] and coupled vibrational states [9, 10] invites state-of-the-art high-dimensional quantum calculations of the molecular eigenstates and

*Corresponding author. Email: msuhm@gwdg.de

ISSN: 0040-5167 print/ISSN 1754-2278 online

DOI: 10.1080/0040516YYxxxxxxxx
http://www.informaworld.com

splittings [11]. Recently, emphasis is shifting away from the ground state tunneling splitting [12–20], which is experimentally characterized to more than 8 significant digits [5]. The variation of this splitting with vibrational excitation is found to be a far more facetted test case. Like in the cases of aniline [21] and the HF dimer [3], the dependence of the splitting on the excitation state is an outstandingly sensitive measure for both the quality of the underlying potential energy hypersurface [16, 22] and the rigor of the nuclear quantum dynamics treatment [23]. For malonaldehyde, a large number of theoretical predictions for this dependence [11, 24–32] contrasts with a limited amount of experimental evidence. This also has to do with the lack of a suitable UV chromophore for double resonance experiments [33]. Beyond an estimate for a skeletal mode based on gas phase spectra [10] and a high resolution diode laser jet study of another mode [34], some splittings have been determined from a combined jet, nanomatrix and matrix isolation IR study [35]. Augmentation of the IR spectroscopy data by spontaneous Raman scattering has turned out to be essential for the assignment of more complex cases [36]. Quenching of the splitting in a matrix environment [35–38] can also assist the identification of tunneling pairs. This combination of jet and matrix spectroscopy builds on and goes beyond traditional normal mode analysis of the vibrational spectra [39, 40].

It is the goal of the present work to extend the experimental data base of tunneling splittings from currently 8 [10, 34–36] to 18 vibrationally excited states. The lower frequency excitations should already be within reach of the most accurate quantum dynamical treatments [11], whereas the higher excitations are likely to remain a challenge for accurate theory in the near future. However, our experimental data set can also be used to judge the limits of more simplified and therefore up-scalable approaches [26, 28–31].

Ultimately, our experimental data set will provide important experimental constraints on the width and height of the electronic barrier between the two degenerate minima [41]. Up to now, it has been difficult to bring together in a rigorous way effective, adiabatic barriers derived from microwave and infrared studies [8, 10] and electronic barriers derived from quantum calculations [16, 22, 41–43]. In a coupled system, reduced-dimensionality treatments must always yield effective potentials which encode zero point energy effects from orthogonal degrees of freedom. Only by exploring the phase space in these orthogonal directions, one can rule out that a match between theory and experiment for the ground state tunneling splitting [22, 41] profits from coincidental error compensation between different parts of the potential energy hypersurface.

In a two state time-dependent picture, the tunneling splitting $\Delta\tilde{\nu}$ of the vibrational eigenstates of malonaldehyde can be translated into a pendular motion of the hydrogen atom between the two oxygens or, rather, its periodic emergence/disappearance at the two binding sites, with period $t_p = 1/(c_0 \times \Delta\tilde{\nu})$, where c_0 is the speed of light [36]. Vibrational excitation can drive this period above or below the ground state value of 1.5 ps, depending on how the vibrational displacements support or inhibit the concerted motion of the proton and the π-conjugated OCCCO frame. With increasing excitation, the two state approximation starts to break down due to resonances and the time dependent evolution deviates more quickly from simple periodicity. At room temperature in solution, the incoherent tunneling rate becomes the primary observable [44, 45]. In the present contribution, we will focus the description on the energy eigenstate picture, but one should always have the dynamical implications in mind.

The other simplified picture we want to propagate is the adiabatic representation of the double minimum potential shown in Figure 2. All vibrations of malonaldehyde are faster than the tunneling process and many are faster than the reaction

coordinate vibration for hydrogen exchange [12, 18, 36]. Therefore, it makes sense to treat vibrational excitations like electronic degrees of freedom [46] in a Born-Oppenheimer-like approximation, defining their own adiabatic potential for the slow hydrogen tunneling process [21]. One should keep the limitations of this approximation in mind, but it is legitimate to think of an increased tunneling splitting in terms of a narrowing and lowering of the adiabatic barrier, and *vice versa*. A record increase was already reported for O–H bending excitation [36] in a combined IR and Raman study. Here, we extend the analysis to the 200–3200 cm^{-1} range. Again, the combination of Raman and IR selection rules in supersonic jets and the quenching of the tunneling by asymmetric matrix embedding [37] are instrumental in securing the spectral assignments. Vibrational matrix effects beyond the quenching of tunneling are surprisingly small for malonaldehyde [35], thus supporting this combined approach, which will be outlined in the next section.

2. Experimental

Malonaldehyde is unstable at temperatures above 0 °C and not commercially available. It was synthesized by acidic hydrolysis of 1,1,3,3-tetramethoxypropane with 1 M HCl solution following the description given by Ref. [47] and stored as its sodium enolate salt. From the sodium salt, fresh (deuterated) malonaldehyde was obtained by protonation with HCl (DCl) in diethyl ether followed by vacuum distillation. For matrix measurements, nearly HCl free malonaldehyde was needed and obtained by long pumping times, accompanied by a noticeable loss of substance. However, jet measurements have higher substance demands. Therefore, a larger amount of HCl impurity was tolerated in the gas phase and jet samples.

2.1. *Raman Measurements*

[Fig. 3 close to here]

Raman measurements were performed with a spectrometer denoted *curry*-jet (from classical unrestricted Raman spectroscopy in a jet, Figure 3, see also Ref. [36, 48, 49]). The setup allows for Raman spectroscopy in the gas phase and in supersonic jet expansions with different effective temperatures. It was loaded with malonaldehyde by flushing a carrier gas (He, Air Liquide 99.996 % or Ne, Linde 99.995 %) through a thermostated saturator (0 °C). Due to the vapor pressure of $\approx$ 1 mbar at 0 °C and the carrier gas pressure of $\approx$ 1.5 bar, the concentration was less than 0.1 %. The mixture was filled into a PTFE coated stainless steel reservoir (4.7 L, 0.6 – 0.8 bar) and from there expanded into a vacuum chamber through a movable slit nozzle (4 × 0.15 mm^2). The chamber was kept at a pressure of 0.6 – 2 mbar by two Roots pumps (500 m^3/h, 250 m^3/h) and a 100 m^3/h rotary vane backing pump. The jet behind the nozzle was crossed by a mildly focussed beam of a frequency-doubled Nd:YVO_4 cw laser (Coherent Verdi V18, $P = 18$ W, $\lambda = 532$ nm). The angle between the polarization plane of the incident light and the scattering plane can be modified by a $\lambda/2$ retarder. By increasing the distance d of the laser beam from the nozzle the molecules suffer more collisions with the carrier gas before scattering the light, leading to a lower effective temperature. Tunneling temperatures estimated from the relative population of the two vibrational ground state levels were found to be low (15 – 30 K). The scattered light was collected at a 90° angle with a camera lens which forms a collimated beam that is led out of the vacuum chamber onto a collecting lens. It was focussed through a Raman edge-filter (L.O.T., OD 6.0, $T > 90$ %, 535.4 – 1200 nm) onto the slit of a Czerny-Turner monochromator (McPherson 2051, $f/8.6$, $f = 1000$ mm, 1200 G/mm grating). The dispersed photons were detected by a liquid nitrogen-cooled back-illuminated CCD camera (PI Acton, Spec-10: 400 B/LN, 1340 × 400 pixel). Jet spectra at nozzle distances of 1 and 3 mm were recorded. In most cases, only the colder 3 mm spectra are shown for clarity. Gas phase spectra were recorded by filling the chamber with 200 mbar malonaldehyde/He mixture at room temperature or, in the case of measurements in the region near the Rayleigh line, by expanding the mixture against a background pressure generated by reducing the pump capacity (stagnation pressure $\approx$ 0.3 bar, chamber pressure $\approx$ 0.2 bar). The latter procedure reduces perturbing rotational lines from air which occur in the low frequency region due to small leaks in the vacuum chamber. The temperature is somewhat lower than the ambient temperature but significantly higher than under jet conditions. Whenever we mention gas phase spectra in the following text, we refer to spectra measured under such ambient or near-ambient conditions.

Some attempts to generate Raman spectra of partially deuterated malonaldehyde

were made, but gas phase spectra suffered from rapid H/D exchange and the contribution by multiple deuteration could not be quantified. We limit the discussion to a few selected cases of strong bands observed in the jet expansion.

2.2. *FTIR Measurements*

In addition to Raman spectra, FTIR gas phase and jet spectra were measured. The substance was prepared as described before and mixed with the carrier gases He (Air Liquide 99.996 %) or He + Ar (Ar: Air Liquide 99.998 %). In contrast to the Raman spectra which were obtained in a continuous jet flow, FTIR spectra were derived from jet pulses with a duration of 135 ms. For this purpose, a mixture of $\approx$ 0.1 % malonaldehyde in He was expanded from a stainless steel reservoir (67 L, 0.7–0.9 bar) through a long, narrow slit nozzle (600×0.2 mm^2) into a vacuum chamber which was connected to a buffer volume of 23 m^3 to compensate for the peak substance throughput. The buffer volume was permanently pumped at 2500 m^3/h. The expansion was crossed by the IR beam of an FTIR spectrometer (Bruker Equinox 55 or IFS 66v/S) with an average cross section of 200 mm^2. The focussing of the IR beam inside the chamber and the re-collimation at the outlet were accomplished with KBr lenses. Behind the outlet, the IR beam was focused onto an MCT detector ($\varnothing$ = 2 mm). 80 kHz FTIR scans were synchronized to the core 100 ms of the gas pulses, allowing for a spectral resolution of $\approx$2 cm^{-1}. The S/N ratio was increased by the use of appropriate bandpass filters. Again, gas phase measurements were realized by filling the jet chamber with a small amount of malonaldehyde in He. For details, see Refs. [35, 49, 50].

2.3. *Matrix Isolation FTIR Measurements*

Matrix isolation spectra were recorded with a spectral resolution of 0.12 cm^{-1}, using a Bruker IFS 66/S FTIR spectrometer working in the transmission-reflection mode. The IR beam was focussed by an off-axis parabolic mirror through a KBr window onto a gold-plated copper block which was kept under high vacuum ($\approx$ 10^{-7} mbar). The reflected IR beam was focussed with another off-axis parabolic mirror onto an MCT detector ($\varnothing$ = 1 mm). The copper block was cooled by a closed-cycle He cryogenerator (Cryomech PT-405) and shielded against thermal radiation. Malonaldehyde was mixed with Ne (99.999 %), N_2 (99.9999 %), Ar (99.9999 %), or Xe (99.998 %) in a vacuum line (malonaldehyde/host $\approx$ 2.5/500). Deposition on the copper block was carried out at 4.3 K (Ne), 20 K (N_2 and Ar) or 35 K (Xe). Spectra were recorded at 4.3 K. For details, see Refs. [35, 49, 51].

3. Spectral Analysis

The IR spectrum of malonaldehyde in the mid and far IR region is well characterized at the vibrational level [9, 10, 37, 38]. Aided by quantum chemical calculations the two latest assignments [39, 40] are quite consistent. Beyond our preliminary report [36], there appear to be no Raman spectra of malonaldehyde reported in the literature, yet. However, a theoretical prediction of the Raman activities is available [52]. We independently calculated the normal modes and their Raman activity at the B3LYP/- and MP2/6-311+G(d) level with the software-package Gaussian 03 [53]. Raman activities A were converted to the scattering cross sections σ' relevant to our experiment (Table 1, see also Supplement).

[Table 1 close to here]

3.1. *General considerations*

There are 15 totally symmetric a' in plane (ip) and 6 a'' out of plane (oop) modes for semi-rigid malonaldehyde in its hydrogen-bonded (chelated) form – the only one of relevance in this work. They can be distinguished in Raman spectra by the depolarization ratio [54]. a'' vibrations only contribute to the spectrum with their polarizability tensor anisotropy. They can be removed to a large extent by subtracting from the standard spectrum (laser polarized perpendicular to the scattering plane) $7/6 = 1.167$ times the spectrum obtained with the laser polarized in the scattering plane [48, 50]. What remains are more or less conserved totally symmetric (a') bands, depending on their degree of polarization.

[Fig. 4 close to here]

Disregarding the individual rotational states which sit on top of the vibrational tunneling states and can not be resolved with our setups, four vibrational tunneling transitions exist for each vibration. Phenomenologically, we label the vibrational tunneling states according to their energetic order with an l for the lower component and a u for the upper component. The number 0 is added as an upper index to indicate the vibrational ground state, or 1 to indicate a vibrationally excited state. The right side of Fig. 4 summarizes our nomenclature in a level scheme. As the ground-state tunneling splitting $\Delta\tilde{\nu}^0$ is known [5], the proper assignment of any two transitions which end in different tunneling states of the same vibration is sufficient to calculate $\Delta\tilde{\nu}^1$. However, such an assignment is not always unambiguous and it is better to have redundant information. Two transitions differing by $\Delta\tilde{\nu}^0$ are likely to end in the same excited state level and if an intensity-related second pair is found nearby, its separation from the first pair leads to the excited state splitting $\Delta\tilde{\nu}^1$. To compare to our low resolution spectra, we round $\Delta\tilde{\nu}^0$ to 22 cm^{-1}. Rotational contours in the gas phase IR spectrum can be helpful in supporting the assignment for ip (a') modes [10], whose transition moment will in general lead to an a/b-type hybrid band. Depending on the non-rigid molecular symmetry, there are either two central a-type bands flanked by two b-type bands or *vice versa* (bottom and top on the left side of Fig. 4). Oop-modes show c-type rotational profiles, as the transition dipole vector points along the c axis of inertia (Fig. 1). We will classify the experimental assignments accordingly, based on IR rotational profiles. For ip modes, assignments where the signals alternate from low to high frequency in a- and b-type profile are ruled out. At room temperature, in the limit of small splittings, similar transition moments, and in the absence of resonances, we assume comparable intensities for the transitions $u^1 \leftarrow u^0$ and $l^1 \leftarrow l^0$ as well as for $u^1 \leftarrow l^0$ and $l^1 \leftarrow u^0$, respectively. This is due to the Boltzmann population ratio $\approx 0.9:1$ for the tunneling states l^0 and u^0 and causes relatively

symmetric patterns with characteristic doublet-structures in the gas phase spectra shown in Figure 5. Depopulation of the u^0 state at lower temperature in the jet gives smaller intensities for the corresponding transitions. The effective tunneling temperature was found to decrease efficiently ($\approx$ 16 K, see Supplement), enabling us to distinguish between transitions starting in the lower or upper tunneling state of the vibrational ground state. IR rotational band contours can usually no more be resolved at these temperatures.

[Fig. 5 close to here]

Due to the lack of rotational resolution in our spectra, we refrain from classifying the bands according to non-rigid symmetry group labels in the original assignment process. However, this additional information is very valuable as a final check of our assignments also in comparison to theory. Although one could use the M_{S4} labels with explicit parity notation [2], we keep the equivalent C_{2v} transition state notation [10, 11] for consistency with the malonaldehyde literature. a' vibrations split into a_1 and b_2 tunneling levels and in the absence of perturbations, the a_1 level is lower in energy for vibrations which correlate with totally symmetric displacements at the hydrogen transfer transition state (a_1 vibrations). For b_2 vibrations, the lower tunneling level has overall b_2 symmetry and the upper level a_1 symmetry, due to antisymmetry with respect to C_2 rotation for both the vibrational and the tunneling coordinate. This leads to the separation of a- and b-type rotational contributions on the wavenumber axis for large tunneling splittings, as discussed before. If the IR rotational contour of the inner transitions ($l^1 \leftarrow l^0$ and $u^1 \leftarrow u^0$) is of $a(b)$-type, the fundamental has b_2 (a_1) symmetry [10]. The opposite is true for the outer transitions ($u^1 \leftarrow l^0$ and $l^1 \leftarrow u^0$). For a'' vibrations, the distinction between b_1 and a_2 fundamentals in the C_{2v} molecular symmetry group is less helpful for our purpose, as both give rise to c-type IR profiles. Note, however, that the correlation between normal mode description for ground state vibrations and normal mode description for transition state vibrations is not always unambiguous, as the character of the vibration may change along the tunneling path.

Raman spectra contribute importantly to the assignment for a number of reasons. First of all, they provide access to lower wavenumber regions without loss of sensitivity. Secondly, the intensity ratio between a and b components is now governed by the polarizability derivative tensor, which differs from the transition dipole vector orientation. Therefore, even though there are no exclusion rules for C_s symmetry, different intensity patterns make it more likely to observe all four transitions associated with a given fundamental.

We measured FTIR spectra of malonaldehyde embedded in Ne, Ar, Xe and N_2 matrices. Matrix embedding has the effect of quenching the tunneling splitting [37] and can thus be used to validate the assignments [35]. Due to the surprisingly small matrix effects on the vibrational band centers, this is more or less equivalent to a collapse of the 2-4 transitions into a single band close to the center, sometimes structured by site-splittings. Unless specified otherwise, we restrict the discussion to Ar matrices, but the remaining matrix spectra largely support our assignments, as shown in the Supplement.

With these qualitative patterns in mind, we can now start to analyze the malonaldehyde spectra from low to high wavenumber.

3.2. *Low frequency region*

[Fig. 6 close to here]

In the low frequency region, only Raman gas phase (Fig. 6 a) and jet spectra (Fig. 6 b, c) are reported, without the aid of far-IR jet measurements which are

challenging in this range [55]. The assignment in this region is therefore more tentative than in others, but it introduces the potential ambiguities which can be overcome at higher wavenumber by the Raman/IR [36, 49, 50] and jet/gas phase/matrix complementarities [35, 49]. We start the discussion of the spectra in the region 240–280 cm^{-1} where calculations predict two normal modes (Tab. 1), an oop bending motion of C_cH ($\gamma\, C_cH$) and an ip ring-deformation mode which is commonly referred to as $\nu O\cdots O$ in the literature, because it modulates the $O\cdots O$ distance and should promote tunneling.

The broad gas phase band at $\approx$260 cm^{-1} is depleted in the depolarization experiment (see Supplement), leading to its assignment to the oop mode $\gamma\, C_cH$ and leaving only the peak at 241 cm^{-1} for the assignment to $\nu O\cdots O$. Peaks marked with asterisks are due to rotational transitions of HCl impurities and serve to verify the calibration [56] (see Supplement). Notably, the sharp signal with $\tilde{\nu}$ = 241 cm^{-1} does not relax in the jet spectra. Therefore it is assigned to a transition originating in the l^0 state of malonaldehyde. This is consistent with a pronounced gas phase IR peak at 220 cm^{-1} reported by Smith *et al.* [9], shifted by $\Delta\tilde{\nu}^0$ from the Raman signal, *i. e.* starting at u^0 and ending in the same upper level.

If the 241 cm^{-1} peak corresponds to the transition $l^1 \leftarrow l^0$, a similarly sharp $u^1 \leftarrow u^0$ transition is expected at >220 cm^{-1} in the gas phase. None is found at a reasonable distance, leaving the possibilities of an unlikely perfect overlap with the $l^1 \leftarrow l^0$ transition or a very large excited state splitting. If, on the other hand, the observed Raman signal is due to the transition $u^1 \leftarrow l^0$, the absence of a corresponding transition $l^1 \leftarrow u^0$ in the displayed range below 220 cm^{-1} implies that it is even below $\tilde{\nu}$ = 180 cm^{-1}, poorly accessible in our experiment due to perturbing rotational lines from air. Thus, judging from the Raman data alone, the $\nu O\cdots O$ excited state tunneling splitting is either larger than 40 cm^{-1} or else it is equal to $\Delta\tilde{\nu}^0$. Smith *et al.* list two "definite sharp peak[s]" (not shown in the published spectra) at 157 and 184 cm^{-1}. If one of these peaks has an intensity comparable to the 220 cm^{-1} signal it may be interpreted as the corresponding tunneling transition $l^1 \leftarrow l^0$. This leads to a tunneling splitting $\Delta\tilde{\nu}^1(\nu O\cdots O)$ of either 84 or 57 cm^{-1}, in line with indirect microwave hot band evidence cited in Ref. [9]. The fourth transition $l^1 \leftarrow u^0$ would then be expected to show up in Raman gas phase spectra at 135 or 162 cm^{-1}. We can definitely rule out a signal at 135 cm^{-1} between the air impurities and the N_2 rotational transition at 162 cm^{-1} does not show an anomalously high intensity (see Supplement). The $\nu O\cdots O$ origin of the IR signals at 157 and 184 cm^{-1} is thus somewhat unlikely. Furthermore, this interpretation leads to the IR rotational profile shown in the bottom trace of Fig. 4 (central *a*-type bands, b_2 symmetry [10]). This is not what one would expect for a vibration whose transition dipole moment lies along the C_{2v} axis in the transition state. However, we can not dismiss an excited state tunneling splitting of 57 cm^{-1} based on this circumstantial evidence.

Still, we tentatively propose an alternative, rather spectacular assignment. If one accepts a very large acceleration of tunneling in this $O\cdots O$ modulation mode, the sharp Raman band at 484 cm^{-1} (Fig. 6) could be the $u^1 \leftarrow u^0$ counterpart of an $l^1 \leftarrow l^0$ transition at 241 cm^{-1}. It appears to relax from 1 mm to 3 mm nozzle distance but not as much as normally expected for a u^0 assignment. However, the predicted IR partners at 220 cm^{-1} ($l^1 \leftarrow u^0$) and 506 cm^{-1} ($u^1 \leftarrow l^0$) are both present as strong Q branches [9]. This would be fully consistent with a totally symmetric $\nu O\cdots O$ vibration (a_1) with a very large $\Delta\tilde{\nu}^1$ splitting of 265 cm^{-1} and weak *b*-type IR components. The 506 cm^{-1} assignment would duplicate the interpretation of a δ ring vibration, though (see below). The effective band center corrected for tunneling would be near 363 cm^{-1}. The enormous size of the postu-

lated splitting could explain the somewhat anomalous relaxation behavior of the 484 cm^{-1} band. As it must be very sensitive to excitation of bath states, the hot bands will be widely spread and jet cooling leads to both, a replenishing of the vibrationally cold $u^1 \leftarrow u^0$ transition and a depletion of the u^0 population. On the other hand, a splitting similar to the fundamental itself is quite unusual and possibly, the 484 cm^{-1} band is rather the overtone of the 241 cm^{-1} fundamental [32].

Due to the unfortunate constellation of missing IR jet data, incomplete Raman coverage, poor signal-to-noise ratio and large splitting, we have to leave this assignment open. However, each of the two tentative assignment proposals is consistent with a large excited state splitting. The most accurate prediction for $\Delta\tilde{\nu}^1(\nu\mathrm{O}\cdots\mathrm{O})$ is 64 cm^{-1} [11], favoring our first assignment. In this case the calculated vibrational-tunneling u^1-level (322 cm^{-1}) overestimates the experimental one (241 cm^{-1}), consistent with the expectations of the authors [11]. In the more spectacular large splitting case, it would underestimate the experimentally inferred u^1 level (506 cm^{-1}). Raman and IR jet measurements beyond the current state-of-the-art will be needed to resolve this assignment ambiguity.

For $\gamma\,\mathrm{C_cH}$ we tentatively assign the centers of the depolarized (a'') bands found in the Raman spectra (273, $\approx$258 cm^{-1}) to the transitions $l^1 \leftarrow l^0$ and $u^1 \leftarrow u^0$, respectively. This is consistent with IR gas phase signals found by Smith *et al.* [9] (282, 252 cm^{-1}), shifted from the Raman signals approximately by the ground state tunneling splitting $\Delta\tilde{\nu}^0$. Based on the behavior of the Raman signals under jet cooling and the shifts of the IR and Raman signals, the IR signals belong to the transitions $u^1 \leftarrow l^0$ (282 cm^{-1}) and $l^1 \leftarrow u^0$ (252 cm^{-1}). Actually, there is weak evidence for the 252 cm^{-1} transition and for a 278 cm^{-1} transition in the Raman gas phase and jet spectra as well. From the transitions $u^1 \leftarrow l^0$ and $l^1 \leftarrow l^0$ follows

$$\Delta\tilde{\nu}^1(\gamma\,\mathrm{C_cH})/\mathrm{cm}^{-1} = 282 - 273 = 9$$

while the transitions $l^1 \leftarrow u^0$ and $u^1 \leftarrow u^0$ yield

$$\Delta\tilde{\nu}^1(\gamma\,\mathrm{C_cH})/\mathrm{cm}^{-1} = 258 - 252 = 6.$$

The deviation among the two estimates reflects some of the uncertainties in the centers of the broad bands. The expected matrix signal (the average wavenumber of all observed IR and Raman transitions) is located at 266 cm^{-1} which matches the IR signal reported by Firth *et al.* [37] at 274 cm^{-1} reasonably well. We note that our assignment is at variance with the assignment proposed by Tayyari & Milani-Nejad [39] who attributed the 282 cm^{-1} signal to the ring-deformation vibration $\nu\mathrm{O}\cdots\mathrm{O}$. Furthermore, we emphasize that this assignment is again less certain than those in the following fingerprint region (Section 3.3).

The Raman gas phase spectrum shows a weak, broad band around 380 cm^{-1}. In the literature there is consistency in placing an oop ring-deformation mode γ ring in this region. Its a'' symmetry is confirmed by our depolarization experiment (see Supplement). Smith *et al.* [9] and Seliskar & Hoffmann [10] found two prominent signals with comparable intensity at 390 [9] (391 [10]) and 384 cm^{-1} in FTIR gas phase spectra. Firth *et al.* reported a matrix signal at $\tilde{\nu}$ = 390 cm^{-1} [37] close to their average wavenumber. Theory predicts a small Raman activity [52] which translates into a small scattering cross section and fits the observed weak intensity. Raman jet spectra reveal very weak signals near 408, 402 and 404 cm^{-1} for nozzle distances 1 and 3 mm, respectively. Their average value 405 cm^{-1} is shifted by $\Delta\tilde{\nu}^0$ from the lower-wavenumber IR peak and its persistence upon cooling leads

to a $u^1 \leftarrow l^0$ assignment. Consequently, the IR signals can be assigned to $u^1 \leftarrow u^0$ (384 cm^{-1}) and $l^1 \leftarrow l^0$ (390 cm^{-1}), giving

$$\Delta\tilde{\nu}^1(\gamma\,\mathrm{ring})/\mathrm{cm}^{-1} = 405 - 390 = 15.$$

Here and in the following, we use the more recent and better resolved IR gas phase spectrum from Smith *et al.* [9] for our calculations. The $l^1 \leftarrow u^0$ transition is predicted at 368 cm^{-1} within the broad gas phase band but too weak to be seen in the Raman jet spectra. A weak IR gas phase signal is found at this position [9] but not the corresponding signal at 405 cm^{-1}.

The next higher-wavenumber fundamental (an a' ring-deformation vibration denoted $\delta\,\mathrm{ring}$), assigned to signals emerging from a rather complex band in IR gas phase spectra [9, 10] at $\approx$ 500 cm^{-1}, may be perturbed by Fermi interaction with a' overtones of the vibrations located at approximately half the fundamental wavenumber, $\nu\mathrm{O}\cdots\mathrm{O}$ and $\gamma\,\mathrm{C_cH}$. Inclusion of large amplitude tunneling symmetry does not increase the number of possible interactions. In this region, there could also be an a'' combination band involving $\gamma\,\mathrm{C_cH}$ and $\nu\mathrm{O}\cdots\mathrm{O}$ [32]. Indeed, adding the wavenumbers of the $l^1 \leftarrow l^0$ transitions (273 cm^{-1} + 241 cm^{-1}) leads to the broad, depolarized, cooling-persistent band observed at 511 cm^{-1}, whose tunneling partner would be difficult to identify. Discounting this band, the Raman spectrum of the gas phase shows at least five weak peaks. Their a' character is confirmed in a depolarization experiment which yields band positions of 484, 492, 521, 527 and 539 cm^{-1}. Upon jet cooling, 3–4 sharp signals survive at 484, 490, 527 and 538 cm^{-1}. At least for the higher wavenumber peaks, the 3 mm jet spectrum suggests the assignment to transitions originating in the l^0 state of malonaldehyde. The observation of more than one Raman active l^0-transition indicates the presence of Fermi resonance. The assumption of $\delta\,\mathrm{ring}$, $l^1 \leftarrow u^0$ for 484 cm^{-1}, together with the second strong IR signal at 512 cm^{-1} [9] (513 cm^{-1} [10]) would demand a strong Raman transition at 534 cm^{-1}, which is not observed. Therefore, the two IR signals at 506 and 512 cm^{-1} have to be connected differently to the Raman peaks observed here. This can be done straightforwardly with the peak at 527 cm^{-1} due to (527 − 506) $\mathrm{cm}^{-1} \approx \Delta\tilde{\nu}^0$. This implies the $l^1 \leftarrow u^0$ transition to appear at 490 cm^{-1}, in agreement with a Raman jet signal which might correspond to the 492 cm^{-1} transition found in the depolarization experiment. However, this signal shows an ambiguous temperature dependence. The average wavenumber of the $\delta\,\mathrm{ring}$ signals at 509 cm^{-1} is close to signals at 510 and 511 cm^{-1} reported for malonaldehyde embedded in Kr- and Ar-matrices [37, 38]. Furthermore, the IR a-type character of the inner transitions is consistent with a transition moment of the vibration along the a-axis when the proton is midway between the oxygen atoms, *i. e.* a b_2 mode in C_{2v} symmetry [11]. From this assignment one obtains the tunneling splitting

$$\Delta\tilde{\nu}^1(\delta\,\mathrm{ring})/\mathrm{cm}^{-1} = 527 - 512 = 15.$$

The same decrease (–6 cm^{-1}) was reported by Seliskar & Hoffmann from evaluation of IR gas phase spectra of parent and deuterated malonaldehyde [10].

The 506 cm^{-1} IR transition thus has two postulated contributions, $u^1 \leftarrow l^0$ for $\nu\mathrm{O}\cdots\mathrm{O}$ and $u^1 \leftarrow u^0$ for $\delta\,\mathrm{ring}$. On the other hand, the signals at 538 cm^{-1} (l^0) and 521 cm^{-1} (u^0) are not connected to any other Raman signal by $\Delta\tilde{\nu}^0$. They may be due to overtone transitions (*e. g.* $2\,\gamma\mathrm{C_cH}$), possibly intensified by Fermi resonance with $\delta\,\mathrm{ring}$. Clearly, there is a strong need for IR jet spectra in this range to unravel the complex tunneling and vibrational dynamics.

3.3. *Fingerprint region*

[Fig. 7 close to here]

We skip the oop mode at 767 cm^{-1} [9, 10, 35] as it has been shown by IR spectroscopy [35] to leave the tunneling splitting unchanged and Fig. 5 reveals no significant Raman intensity. Further Raman signals were observed in the region 800–1200 cm^{-1} (Fig. 7). The Raman gas phase spectrum (d) shows three distinct bands with obvious doublet structures. The intensity pattern, namely two bands with comparable intensities and one with higher intensity in the middle, matches calculated scattering cross-sections (Tab. 1) [52]. The corresponding vibrations are a second ip ring-deformation mode ($\delta\,\mathrm{ring}\,2$) at $\approx$ 880 cm^{-1}, a C–C stretching vibration at $\approx$ 980 cm^{-1}, and an ip bending vibration of the central C_eH segment with some amplitude in a C–O stretching motion ($\delta\,C_eH$) at $\approx$ 1100 cm^{-1}. The IR gas phase spectrum (a) shows two strong bands with at least four Q-branches for the lower-frequency band and two Q-branches for the band at $\approx$ 1000 cm^{-1}.

The common IR/Raman activity in the region around 880 cm^{-1} is actually misleading. In addition to the Raman-active $\delta\,\mathrm{ring}\,2$ mode with little IR intensity, calculations [39, 40, 52] predict an oop OH/C_aH out of phase bending mode ($\gamma\,OH/\gamma\,C_aH$), which is predominately IR-active. The analysis of $\gamma OH/\gamma C_aH$ centered at 893 cm^{-1} has been given before based on gas phase, jet, and matrix IR spectroscopy [35]. It exhibits a very small (3–5 cm^{-1}) tunneling splitting and there is no evidence in the Raman jet spectrum (e) for complementary tunneling transitions.

The $\delta\,\mathrm{ring}\,2$ mode is characterized by its doublet structure in the Raman gas phase spectrum (883, 878 cm^{-1}). The depolarization experiment confirms its ip or a' character. IR counterparts to the Raman doublet are seen to be coincidental (probably $\gamma\,OH/\gamma\,C_aH$ hot bands) when comparing to the jet spectrum (b). The Raman jet spectrum shows that the 878 cm^{-1} band survives and thus corresponds to a transition from l^0. This is sufficient to analyze the tunneling pattern, because the doublet is separated by less then $\Delta\tilde{\nu}^0$. Negative excited state tunneling splittings would result from a $u^1 \leftarrow l^0$ and $l^1 \leftarrow u^0$ assignment. We thus assign 883 cm^{-1} to the transition $u^1 \leftarrow u^0$ and 878 cm^{-1} to the transition $l^1 \leftarrow l^0$, respectively, yielding

$$\Delta\tilde{\nu}^1(\delta\,\mathrm{ring}\,2)/\mathrm{cm}^{-1} = 883 - 878 + \Delta\tilde{\nu}^0 \approx 27.$$

Comparison with available IR matrix data is prevented by $\gamma\,OH/\gamma\,C_aH$ overlap. In this particular case, it is instructive to discuss the results for singly deuterated malonaldehyde (see Supplement). A band at 835 cm^{-1} corresponds to the dominant transition at 878 cm^{-1} in the non-deuterated species. The absence of a separate $u^1 \leftarrow u^0$ band and the width of the 835 cm^{-1} band indicate that the two Raman transitions coincide within the resolution of our experiment. Therefore, the exited state tunneling splitting is close to the ground state splitting of $\approx$ 3 cm^{-1} [8].

Moving closer to 1000 cm^{-1}, quantum chemical calculations [39, 40, 52] predict a C–C stretching vibration (ν C–C) and an in-phase oop bending mode involving OH, C_aH and C_cH. Theoretical intensities indicate that the stretching mode is dominant in Raman [52] and IR spectra [39, 40]. Indeed, both gas phase spectra show clear doublet structures indicative of a single dominant fundamental (IR: 964, 999 cm^{-1} and Raman: 977, 985 cm^{-1}). The IR signal at 999 cm^{-1} was previously assigned to the C–C stretching mode [39, 40]. The signal at 964 cm^{-1} was not assigned in the latest publications. The in-plane assignment is supported by polarization measurements. The IR and Raman signals are connected by the ground state tunneling splitting (999 cm^{-1} – 977 cm^{-1} $\approx \Delta\tilde{\nu}^0$, 985 cm^{-1} – 964 cm^{-1} $\approx \Delta\tilde{\nu}^0$) which

confirms a common vibrational origin. The higher frequency transitions survive in the jet spectra (1000 cm^{-1}, 986 cm^{-1}), corresponding to the tunneling transitions $u^1 \leftarrow l^0$ and $l^1 \leftarrow l^0$, respectively. The temperature-sensitive bands at 978 cm^{-1} (jet) and 964 cm^{-1} (gas phase only) are thus assigned to the transitions $u^1 \leftarrow u^0$ and $l^1 \leftarrow u^0$ yielding an upper state tunneling splitting of

$$\Delta\tilde{\nu}^1(\nu\,\mathrm{C\text{–}C})/\mathrm{cm}^{-1} = \frac{1}{2}\cdot(1000 - 986 + 978 - 964) = 14.$$

The clearcut Raman spectrum allows for a characterization of the effective tunneling level population and thus temperature T_t of the expansions. As shown in the Supplement, expansion in He leads to $T_t = 30$ K at a nozzle distance of 1 mm, whereas Ne expansion at 3 mm distance leads to $T_t = 16$ K. The IR and Raman transitions are nearly complementary, with some evidence for IR *b*-type transitions at the Raman positions. The Q-branches of the IR transitions are compatible with a_1 symmetry. The predicted quenched matrix isolation band is at 982 cm^{-1} which compares perfectly with peak positions reported in the literature at 982 cm^{-1} [37, 38] for Ar matrices. The most intense signal of our complex Ar matrix band lies at 983 cm^{-1}. Finally, the Raman spectrum of the deuterated sample shows the $u^1 \leftarrow u^0$ transition as a shoulder on the low-frequency slope of the $l^1 \leftarrow l^0$ transition at 975 cm^{-1} (see Supplement). A Gaussian curve fit confirms that the tunneling splitting is slightly decreased (1 – 2 cm^{-1}) by the C–C stretching vibration, relative to the vibrational ground state splitting of 3 cm^{-1} [8]. In summary, this is a textbook example for the complementarity of IR/Raman and gas phase/jet/matrix assignments of tunneling in malonaldehyde.

We continue with the Raman signals at 1074 and 1113 cm^{-1}. Quantum chemical calculations and the polarized character of the transitions support the assignment to $\delta\,C_eH$ as mentioned above. Supersonic jet expansion identifies l^0 as the origin of the high frequency signal at 1113 cm^{-1}, whereas the low frequency signal at 1074 cm^{-1} drops in relative intensity and thus originates in u^0. The Raman spectra point at corresponding dips in the IR spectra with the same behavior under jet cooling. The observed signals imply further tunneling transitions, but the experimental match is not perfect and the assignment 1113 cm^{-1} to $u^1 \leftarrow l^0$ and 1074 cm^{-1} to $l^1 \leftarrow u^0$ is already unambiguous. This gives:

$$\Delta\tilde{\nu}^1(\delta\,\mathrm{C_eH})/\mathrm{cm}^{-1} = 1113 - 1074 - \Delta\tilde{\nu}^0 \approx 17$$

and b_2 symmetry. IR matrix signals are found at 1094 cm^{-1} in the literature [37, 38] and in the present work, in perfect agreement with the average wavenumber of the jet signals (1094 cm^{-1}). For this vibration, O-deuteration appears to increase the excited state tunneling splitting from 17 cm^{-1} to about 20 cm^{-1}, judging from two analogous Raman transitions at 1106 and 1083 cm^{-1} in a supersonic jet expansion. Relative to the decreased ground state splitting of 3 cm^{-1}, this corresponds to an increase by one order of magnitude. A straightforward rationalization comes from the theoretical prediction of more OD bending character in the normal mode. As shown before [36] and summarized in the following, this bending motion can increase the tunneling splitting by an impressive amount.

[Fig. 8 close to here.]

The spectral region from 1200 to 1400 cm^{-1} (Fig. 8) was already discussed in depth in a preceding paper [36]. Therefore we will give just a short summary here. Quantum chemical calculations place three X–H bending vibrations in this spectral window, namely ip bending modes of C_aH, OH and C_cH (in this order from low to high frequency). For $\delta\,C_aH$ ($\approx$ 1260 cm^{-1}), no Raman signals were found.

However, the tunneling spitting for the vibrationally excited state could be derived from intense IR transitions indicating b_2 symmetry ($\Delta\tilde{\nu}^1(\delta\,C_aH) = 8$ cm^{-1}). The OH bending mode at $\approx$ 1300 cm^{-1} stands out due its high Raman activity. Its δ OH assignment is complicated by perturbations from combination- or overtones which are selectively activated in one of the excited tunneling levels by local Fermi resonances (marked with $*$). The reason is a large tunneling splitting of 69 cm^{-1} in the dominant δ OH state (a_1) which decouples the interaction partners of the two tunneling levels. The opposite limit is observed for the $\delta\,C_cH$ band at $\approx$ 1400 cm^{-1}. Its IR and Raman signals are shifted by $\approx$ 22 cm^{-1}. With the lower-frequency signal relaxing under jet cooling, this is consistent with a complete quenching of the tunneling process ($\Delta\tilde{\nu}^1(\delta\,C_cH) \approx 0$ cm^{-1}) and prevents an assignment of the non-rigid symmetry species. Other than in Ref. [36] we show matrix spectra with less impurities in Fig. 8. The previously reported Ar matrix signals are observed but not prominent. The broad Ne matrix band is slightly shifted. Variations are within the expected magnitude for matrix site effects. Peak positions listed in Tab. 2 refer to the strongest signals found in the current Ar matrix spectrum.

[Fig. 9 close to here.]

Fig. 9 shows the spectral region from 1500 to 1700 cm^{-1}. The weak IR band at $\approx$ 1450 cm^{-1} (Fig. 5) is not supported by Raman signals, but its excited state tunneling splitting has been analyzed before based on our IR work [35]. The most intense band in both, IR and Raman spectra ($\approx$ 1600 cm^{-1}), belongs to an in-phase C=C/C=O stretching vibration. This is well confirmed by quantum chemical calculations [39, 40, 52]. It was in the focus of a former high-resolution lead salt diode laser jet study [34] which revealed a reduction by just 0.03 cm^{-1} for the tunneling splitting in the vibrationally excited state, *i. e.* leaving the proton transfer essentially unchanged. We discuss it here from a low resolution perspective. Instead of the characteristic doublet structure there is just one strong *a*-type band in the FTIR spectra (1593 cm^{-1} gas phase, 1594 cm^{-1} jet [35]). It is caused by the superimposed transitions $u^1 \leftarrow u^0$ and $l^1 \leftarrow l^0$. This assignment implies the two transitions $l^1 \leftarrow u^0$ and $u^1 \leftarrow l^0$ being shifted by $\approx \pm$ 22 cm^{-1}. Indeed, strong signals at 1573 and 1615 cm^{-1} are found in the Raman jet spectra and show the expected cooling behavior. Corresponding IR *b*-type bands may be guessed in particular near 1614 cm^{-1}, in line with a b_2 fundamental interpretation. As in the case of δ OH, there are some peaks (marked with asterisks) stealing intensity from the $u^1 \leftarrow l^0$ transition, indicative of u^1-specific Fermi resonances. It would be rewarding to analyze them at high resolution [34], as they appear to differ in their tunneling splitting. The matrix spectrum shows a broad and slightly split band with its peak position at 1592 cm^{-1}, close to the average gas phase- and jet signal positions. In conclusion, the observations made for this band agree with the high resolution findings.

FTIR spectra show a weaker band at $\approx$ 1650 cm^{-1} which keeps a complicated structure under jet cooling and matrix isolation. It belongs to an out-of-phase C=C/C=O stretching vibration [9, 10, 39, 40]. The structure of the band may be explained by *b*-type bands at 1637 and 1665 cm^{-1} and an *a*-type band at 1658 cm^{-1}. The weak Raman signals do not fit this IR evidence in a consistent way and are assumed to originate in different transitions. The FTIR signals at 1637 and 1658 cm^{-1} are separated by the ground state tunneling splitting. As the third observed signal lies at a higher frequency and is stable under jet cooling, we assign $u^1 \leftarrow l^0$ to 1665, $l^1 \leftarrow l^0$ to 1658, and $l^1 \leftarrow u^0$ to 1637 cm^{-1}, consistent with b_2 symmetry. The weakness of the fourth expected transition $u^1 \leftarrow u^0$ at 1643 cm^{-1} may be explained by resonances in the u^1 state. The tunneling splitting

in the vibrationally excited state

$$\Delta\tilde{\nu}^1(\nu\,\mathrm{C{=}O}/\nu\,\mathrm{C{=}C\ oph})/\mathrm{cm}^{-1} = 1665 - 1658 = 7$$

must be considered more tentative than others. The matrix spectrum shows a band consisting of two well separated major signals with peak positions at 1649 cm^{-1} (close to the $u^1 \leftarrow l^0$ and $l^1 \leftarrow u^0$ average position, 1651 cm^{-1}) and at 1657 cm^{-1}.

3.4. *CH stretching region*

[Fig. 10 close to here.]

The remaining signals lie in the spectral region 2700 – 3200 cm^{-1} (Fig. 10). This is expected to be a very difficult region due to the near degeneracy of the three CH and the OH oscillator, which may redistribute their spectral intensity and could involve substantial mode couplings, as usual in strong hydrogen bonds [57]. Therefore, our conclusions will remain very tentative and call for more sensitive experiments. Raman and FTIR spectra show no obvious doublets which complicates the determination of $\Delta\tilde{\nu}^1$. Rotational-vibrational transitions from HCl impurities (marked with $*$) dominate the FTIR jet spectrum (b), leaving five transitions which may possibly be assigned to malonaldehyde, located approximately at 2790, 2860, 2870, 2880, and 2910 cm^{-1}. In the case of the Raman spectra (d, e) the HCl signals are less pronounced beyond the Q-branch at 2884 cm^{-1} [58] (marked with $*$). Although the OH-stretching mode is predicted slightly below 3000 cm^{-1} [59, 60], its expected [61, 62] homogeneous width of several 100 cm^{-1} precludes detection in our supersonic jet and even matrix isolation experiments. CH stretching bands are potentially more narrow. While the gas phase spectrum is very complex, there are just two Raman peaks (2863, 2872 cm^{-1}) and one broader structure ($\approx$ 3100 cm^{-1}) surviving the jet cooling. The weakness of the FTIR counterpart to the 3100 cm^{-1} band forces us to concentrate on the up to two Raman active fundamentals near 2900 cm^{-1}. Compared to the predicted Raman cross section (Tab. 1), the observed signals are surprisingly weak (Fig. 5), but this effect might stem partly from the wavelength-dependent sensitivity of the setup. Although there is consistency in the literature in locating the C_cH stretching vibration at 2858 cm^{-1} [9, 10, 39, 40], we refrain from an explicit local mode assignment in this strongly coupled case, which is further complicated by exchanging the role of C_cH and C_aH along the tunneling coordinate, with potentially large diabatic coupling effects.

There is evidence from the Raman jet spectra for an l^0 transition at 2863 cm^{-1}, which seems to correspond to a dip in the IR spectrum, confirmed by the absence of pronounced Q-branches. A nearly unshifted signal is found in case of the Ar matrix spectrum (2864 cm^{-1}) which would suggest a more or less unchanged excited state tunneling splitting ($\approx$ 22 cm^{-1}) and coincident $l^1 \leftarrow l^0$ and $u^1 \leftarrow u^0$ transitions. However, the matrix signal is rather weak and might stem from residual diethyl ether. The l^0 transition changing the tunneling symmetry is obscured by the HCl band center in the Raman spectrum. In the FTIR jet spectrum, the small peak at 2882 cm^{-1} is close to the expected position, but with a shift of 19 cm^{-1} rather than $\Delta\tilde{\nu}^0$, we do not assign it to the $u^1 \leftarrow l^0$ transition. If this very tentative assignment is correct, it demands a_1 symmetry for the underlying CH-stretching mode, due to the b-type character of the IR transitions, and we thus call it ν CH-a_1.

The nearby Raman transition at 2872 cm^{-1} behaves differently. It has a relaxing partner at 2847 cm^{-1} and both Raman bands seem to have weak b-type counterparts in the IR, but again no substantial Q-branch contributions nearby. The only joint physical assignment leads to an excited state tunneling splitting of 3 cm^{-1}

($l^1 \leftarrow u^0$ at 2847 and $u^1 \leftarrow l^0$ at 2872 cm^{-1}). Again, the expected matrix feature falls in the 2860 cm^{-1} range, where only a weak pattern is observed. Here, we must invoke b_2 symmetry, leading to the label ν CH-b_2. This tentatively brings four CH stretching levels into close vicinity (2863 cm^{-1} (a_1), 2885 cm^{-1} (b_2), 2869 cm^{-1} (b_2), 2872 cm^{-1} (a_1)).

The dominant CH-stretching signals in the Ar matrix spectrum at $\approx$2887 cm^{-1} are left unassigned, also considering the rather irregular behaviour with matrix change (see supplement, Fig. S 5), and adding to the exploratory character of our assignment. This constellation demands for a high-resolution investigation, which is, however, particularly challenging at this high energy.

This concludes our spectral discussion. All assignments and tunneling splittings are summarized in table 2.

[Tab. 2 close to here.]

4. Discussion

In the following, the assigned vibrations shall be discussed with respect to their effect on the hydrogen transfer. We will also provide a comparison to theoretical predictions which is summarized in Table 3. Again we move from low to high frequency, but first the overall quality of our experimental approach will be assessed.

The FTIR gas phase and jet spectra were recorded with a resolution of 2 cm^{-1}, while the resolution of the Raman spectra is about 1 cm^{-1}. In favorable cases, the accuracy of experimentally derived tunneling splittings may approach 1 cm^{-1}, but typically the various uncertainties will add to 2–3 cm^{-1}. Exceptions are made explicit in Table 2 and in some cases the assignment itself remains tentative. The wavenumber precision of the matrix spectra is better than 1 cm^{-1} but in addition to the desired quenching of the tunneling splittings, the cryogenic matrix environment may induce shifts and site splittings of several cm^{-1}. Matrix positions are thus used to verify, but not to narrow down the value of the splitting. In the presence of anharmonic perturbations, only the dominant eigenstates are usually analyzed quantitatively. Due to an increased influence of couplings at high wavenumber and a lack of jet FTIR data at low wavenumber, the fingerprint region assignment involves the highest confidence level.

The least ambiguous comparison between experiment and theory would be at the individual $\Gamma_{C_{2v}}$ tunneling-vibrational eigenstate level with a fully converged, full-dimensional quantum dynamics calculation on an accurate full-dimensional surface [16]. As this is not yet feasible beyond the first two levels [18, 19], we compare to the best approximations to this ideal [11, 32], to semiclassical calculations [26, 28], to reaction path/surface approaches [29, 31] and also to intuitive reasoning based on the coupled nuclear motion in normal modes around the local C_s minima. The latter approach has limitations. Even the connection to normal modes around the C_{2v}-symmetric transition state for hydrogen transfer is not always clear. Anharmonic effects and PES imperfections (in our case usually MP2/6-311+G(d), Fig. 1) can change the situation in a qualitative way. Nevertheless, this intuitive approach is appealing due to the insight it offers, when it works.

[Tab. 3 and Fig. 11 close to here.]

For νO$\cdots$O the experimental evidence points to a strongly increased excited state splitting (either +35 or +243 cm^{-1}) which can be rationalized by the periodic shortening of the O–H$\cdots$O distances, leading to a reduced effective barrier height [11, 26]. The increased tunneling splitting is consistently predicted from theory [11, 26, 28, 31, 32] and must be considered qualitatively robust. When it comes to quantitative prediction, things are much less clear. A splitting enhancement by 243 cm^{-1} is not predicted by any theoretical model, whereas the experimental alternative of 35 cm^{-1} is more in line with the most sophisticated predictions [11, 32]. The quality of the experimental data is not sufficient to challenge theory in this case, just to inspire further work. The excitation of $\gamma\,C_cH$ leads to a decrease of the tunneling splitting by 13 to 16 cm^{-1} because the carbonylic oxygen moves out of the molecular plane, increasing the average OH$\cdots$O distance (Fig. 11). Theoretical predictions range from tunneling splittings higher than the ground state splitting [31] to minor changes [26, 28] or a decrease by 7.2 cm^{-1} [29], 10.9 cm^{-1} [32] and 16.8 cm^{-1} [11]. Here, the best theoretical predictions and the somewhat uncertain experimental band localizations are rather balanced and improved spectral resolution and signal strength would be needed to challenge theory. For the oop ring-deformation vibration γring, the mechanism is similar, as the OH-fragment bends out of the molecular plane which causes a reduced tunneling splitting (–7 cm^{-1}). Surprisingly, most of the available calculations predict an

increase of the tunneling splitting [26, 28, 29, 31], except the recent calculations by Hammer *et al.* (–17.3 cm^{-1} [32], –7.2 cm^{-1} [11]). The variation in sequence between $\gamma\,C_cH$ and γ ring among the full-dimensional predictions [11, 32] suggests some sensitivity to the employed potential energy hypersurface [16, 22]. The ring-deformation vibration δ ring is a case where the normal mode mainly alters the bond angles but not the distances. The observed decrease of the tunneling splitting (–7 cm^{-1}) can not be rationalized straightforwardly by normal mode analysis. The value from Seliskar & Hoffmann (–6 cm^{-1}) was confirmed within the error of our experiment, but, due to resonances, the spectral situation is not unambiguous. Theoretical predictions show a wide variation of results, ranging from a complete quenching of the tunneling process [31] to a substantial increase [29]. The small changes of the tunneling splitting calculated by Hammer *et al.* (–6.4 cm^{-1} [32], –4.7 cm^{-1} [11]) come very close to the experimental value.

Coming now to the experimentally most robust determinations, the $\approx$ 880 cm^{-1} δ ring 2 deformation vibration increases the tunneling splitting by 5 cm^{-1}. The corresponding normal mode alters the HO–C=C and O=C–C angles in phase while the central C_eH fragment moves towards and away from the ring (Fig. 11). By OH-bending, the OH$\cdots$O distance is temporarily shortened when the C_eH fragment approaches the ring center. Theory is consistent in predicting an acceleration of the proton transfer by this vibration [11, 26, 28, 29, 31] although the predicted magnitude scatters a lot. For the C–C stretching vibration ν C–C the hydrogen transfer is found to decrease by 8 cm^{-1} although this vibration also involves periodic shortening of the OH$\cdots$O distance. This may be rationalized by the C–C bond being stretched during the shortest OH$\cdots$O approach, unfavorable for the electronic rearrangement to a double bond. Only the most recent work by Hammer & Manthe (–8.9 cm^{-1}) [11] predicts the correct effect on the hydrogen transfer. The same is true for $\delta\,C_eH$. Besides C_eH bending the normal mode involves a minor amplitude in the C–O bond stretch but its excitation has only a small effect on the tunneling splitting, which is found to decrease by 5 cm^{-1}.

The C–H bending vibrations in the spectral window from 1200 – 1400 cm^{-1} are not localized and noticeable stretching motion in the molecular backbone and OH bending takes place. The C_aH bending vibration reduces the tunneling splitting by 14 cm^{-1}, in agreement with the smallest OH$\cdots$O distance being realized when the C–O bond is unfavorably stretched. Hammer & Manthe find a somewhat more pronounced decrease of the tunneling splitting by 20.6 cm^{-1} [11] while others predict an increased [26, 28, 29] or an unchanged excited state tunneling splitting [31]. δ OH was discussed in our previous publication [36]. The OH bending motion is accompanied by concerted nuclear displacements favorable to the electronic rearrangement. Most predictions are in agreement with the observed increase (+47 cm^{-1}) but only Benderskii *et al.* (+510.5 cm^{-1}) [28] and Hammer & Manthe (+60.1 cm^{-1}) [11] confirm the outstanding impact of δ OH excitation. The complete quenching of the hydrogen transfer by the following $\delta\,C_cH$ vibration (which is quite similar to δ OH) can not be easily rationalized. A small increase of the tunneling splitting is consistently and erroneously predicted from theory [26, 28, 29, 31].

The in-phase C=O/C=C stretching vibration was studied at high resolution [34] and our complementary measurements confirm the mainly unchanged excited state tunneling splitting. When the frame displacement favors the bond transformation taking place along with the hydrogen transfer, the OH bending increases the OH$\cdots$O distance. These two effects seem to balance each other. Comparing this result to the finding for δ OH emphasizes the need for concerted framework displacements during the hydrogen transfer process. Predictions vary for this vibration. Comparison of our results for the in-phase and out-of-phase C=O/C=C

stretching vibrations to results from Hammer & Manthe is not unambiguous in this case, due to potential mode switches along the tunneling coordinate. For the out-of-phase vibration which involves less OH bending we find the excited state tunneling splitting to decrease by 15 cm^{-1}. During hydrogen bond shortening, the C=C bond is unfavorably compressed. Smaller decreases are found by Meyer & Ha (–2.4 cm^{-1}) [29] and Hammer & Manthe (–4.7 cm^{-1}) [11].

The CH stretching assignments remain very tentative due to sparse experimental evidence and expected couplings within the CH manifold and to the OH stretching mode, as outlined before. Here, a reduced dimensionality model of the four hydride stretches may offer important insight, as would improved experimental spectra. Potentially, quite spectacular effects may occur, as indicated by some of the tunneling predictions [28].

[Fig. 12 close to here.]

In Figure 12, the overall picture for the new and previously known tunneling splittings below 1800 cm^{-1} is summarized and compared to recent predictions. Not unlike the case of tropolone [33], a'' modes tend to reduce the tunneling splitting and so does a majority of a' modes. For strongly promoting modes, unlike the case of tropolone, there is a danger of losing track of the tunneling partner, when they are too far apart. Nevertheless, evidence for some large splittings could be collected in the present work. In the related acetylacetone case, coupled motion of 7 hydrogen atoms changes the situation dramatically [63].

5. Conclusion

We have investigated the effects of versatile vibrational excitations on the tunneling splitting of malonaldehyde by means of complementary FTIR and Raman spectroscopy in the gas phase, in supersonic jet expansions and in cryogenic matrices. Unlike the related larger cases of tropolone [33] and 9-hydroxyphenalenone [64], malonaldehyde currently offers no other way than direct absorption and Raman scattering to carry out such a study. It was shown that vibrational excitation can have a pronounced impact on the intramolecular hydrogen transfer, reflected by tunneling splittings reaching from 0 to 69 cm^{-1} [36] or even larger values. Generally, vibrational excitation was found to decrease the tunneling splitting. An increase was found for deformation vibrations which involve variation of the OH$\cdots$O-distance and vibrations with OH bending character when they come along with favorable framework distortions anticipating bond order changes. Many of these effects can be rationalized qualitatively by elementary discussion of simple MP2/6-311+G(d) normal modes. When it comes to quantitative predictions, we could show that only the latest work on multiconfigurational time dependent Hartree calculations on full-dimensional potential energy hypersurfaces [11, 32] has so far been able to make reliable, systematic forecasts about the extent to which a certain excitation promotes or inhibits the periodic hydrogen motion through the double minimum barrier. While the accuracy of fundamental band center predictions leaves room for improvements, the prospects for a theoretical description of multidimensional aspects of proton tunneling look bright. As a next theoretical step, it would be helpful to apply different quantum dynamical approaches to the best full-dimensional hypersurface [16] to separate the effects of electronic and nuclear dynamics approximations. Now that we have extended the experimental database to nearly 20 mode-dependent splittings, malonaldehyde appears to be the ideal molecular meeting point between quantum chemistry, quantum dynamics, and vibrational spectroscopy of hydrogen transfer [44] between two equivalent sites. To cite a referee – this is a molecular system that will continue to tease experimentalists and theoreticians for many years to come.

Acknowledgements

The experimental work was part of the diploma thesis of N. Lüttschwager (2009) and we thank D. Luckhaus for triggering the preceding FTIR study during his stay in Göttingen. This work is dedicated to Martin Quack on the occasion of his 65th birthday to honour his passion for quantum tunneling, but falling short of his passion for high spectral resolution, which could help to resolve some of the open questions presented here.

Figures

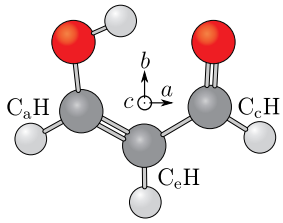

Figure 1. Structure of enolic malonaldehyde, optimized on the MP2/6-311+G(d) level. *a*, *b*, *c* refer to the primary axes of inertia. The CH fragments are denoted C_cH for the carbonylic, C_eH for the enolic, and C_aH for the alcoholic CH fragment.

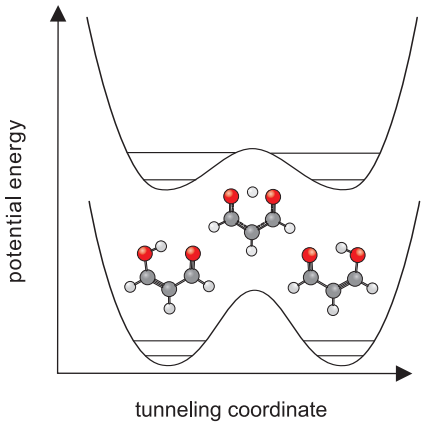

Figure 2. Illustrative adiabatic potentials for the description of hydrogen transfer in malonaldehyde in the vibrational ground state (lower curve) and in a hypothetical vibrationally excited state (upper curve) which promotes hydrogen tunneling as a consequence of the lower barrier.

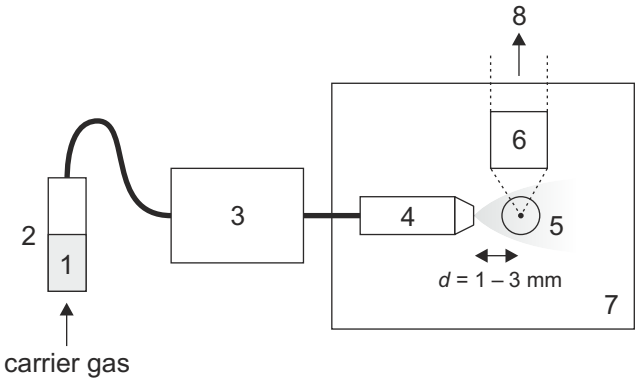

Figure 3. Sketch of the *curry*-jet setup; 1 – substance, 2 – thermostated saturator, 3 – pre-expansion reservoir, 4 – nozzle, 5 – focused laser beam (perpendicular to image plane) & lens, 6 – camera lens, 7 – vacuum chamber, 8 – monochromator equipped with N_2 cooled CCD

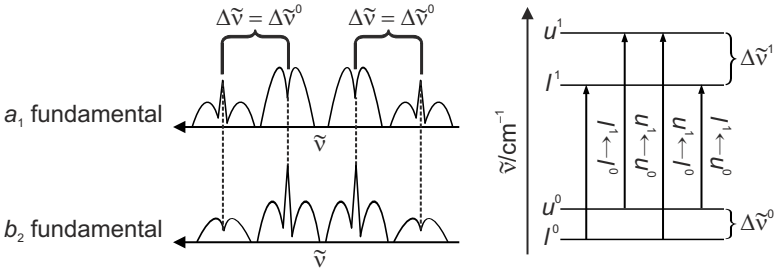

Figure 4. Possible sequences for IR rotational profiles of ip vibrational transitions (left) and underlying energy level scheme for the assignment of vibrational-tunneling transitions of malonaldehyde (right). The first two and the last two transitions in the scheme should show comparable intensity in ambient gas phase spectra, respectively, if the excited state splitting is not too large and the vibrationally excited states are not involved in anharmonic couplings.

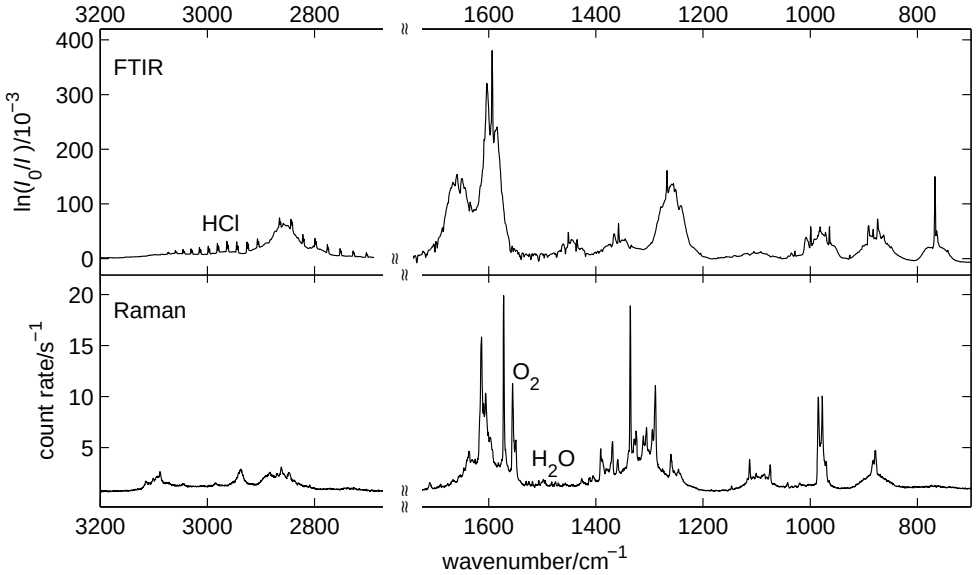

Figure 5. FTIR and Raman gas phase spectra of malonaldehyde. In the 1700–2700 cm^{-1} region no strong signals were found. Between 1400 and 1700 cm^{-1} water impurities are observed.

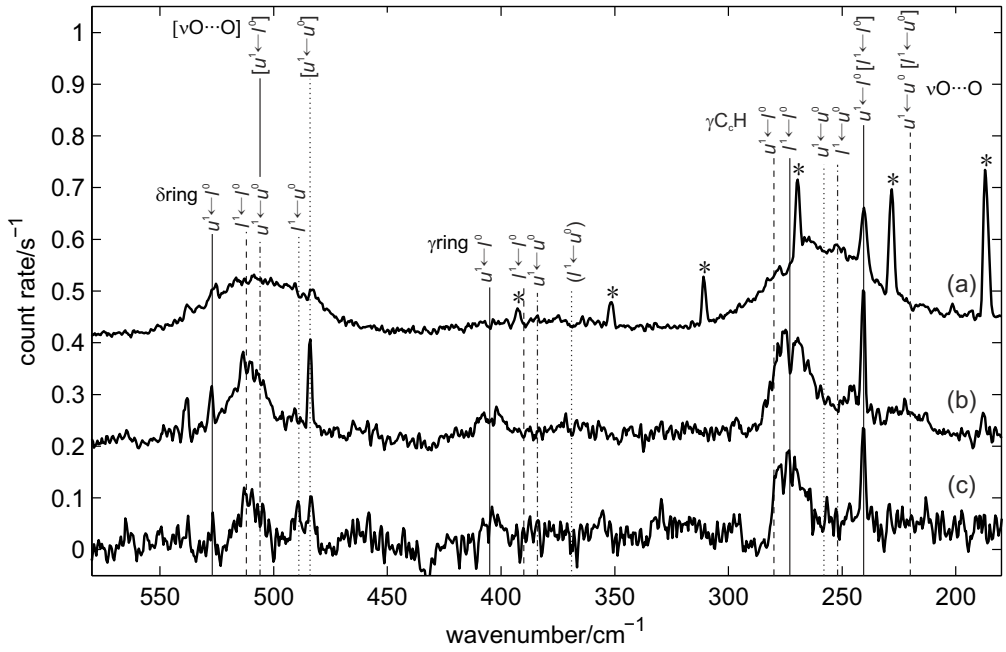

Figure 6. Raman gas phase and jet spectra of malonaldehyde in the region 200–550 cm^{-1}; (a) gas phase spectrum ×0.13, (b) 1 mm jet spectrum ×0.4, (c) 3 mm jet spectrum; assignments are indicated with solid lines for Raman active l^0 transitions, dotted lines for Raman active u^0 transitions, dashed lines for IR active l^0 transitions, and dash-dotted lines for IR active u^0 transitions [9, 10]. The alternative $\nu\mathrm{O}\cdots\mathrm{O}$ assignment is given in square brackets. Rotational lines from residual HCl are marked with ∗.

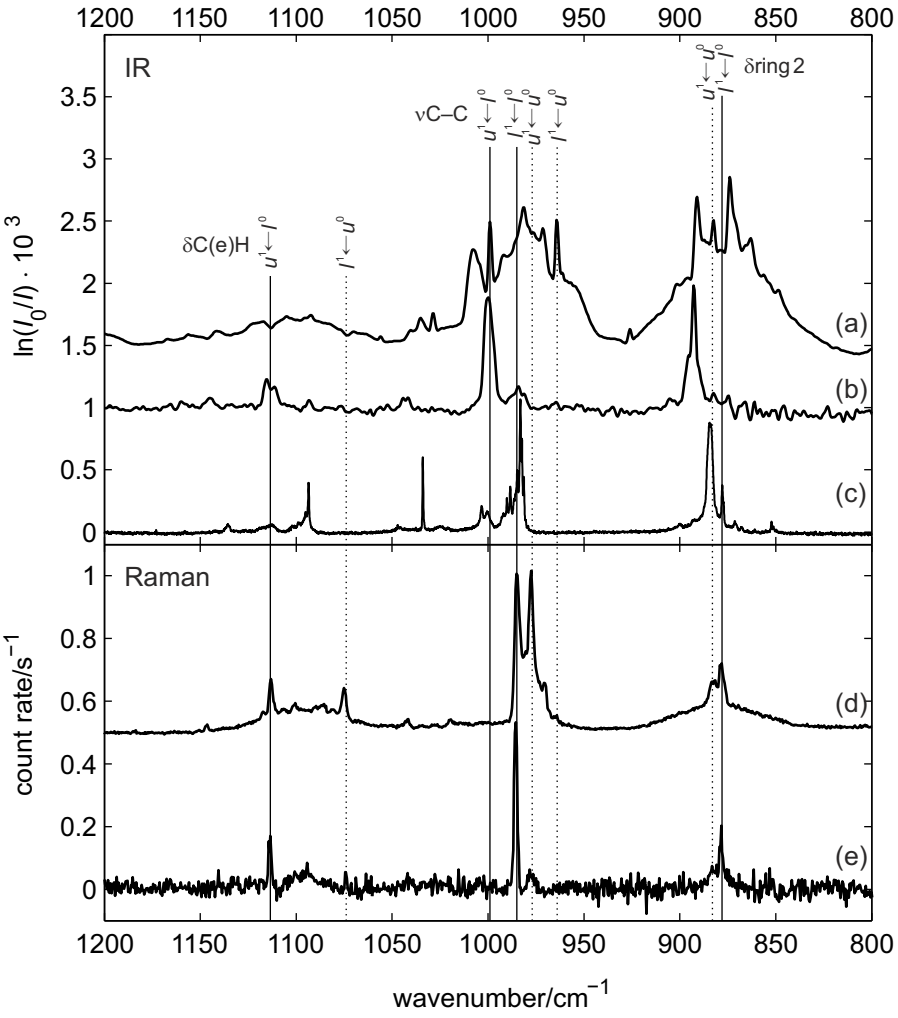

Figure 7. Vibrational spectra of malonaldehyde in the region 800 – 1200 cm^{-1}; (a) FTIR gas phase spectrum $\div 20$, (b) FTIR jet spectrum, (c) FTIR Ar matrix spectrum $\div 500$, (d) Raman gas phase spectrum $\div 18$, (e) 3 mm Raman Ne jet spectrum; assignments are indicated by solid lines for l^0 transitions and dotted lines for u^0 transitions.

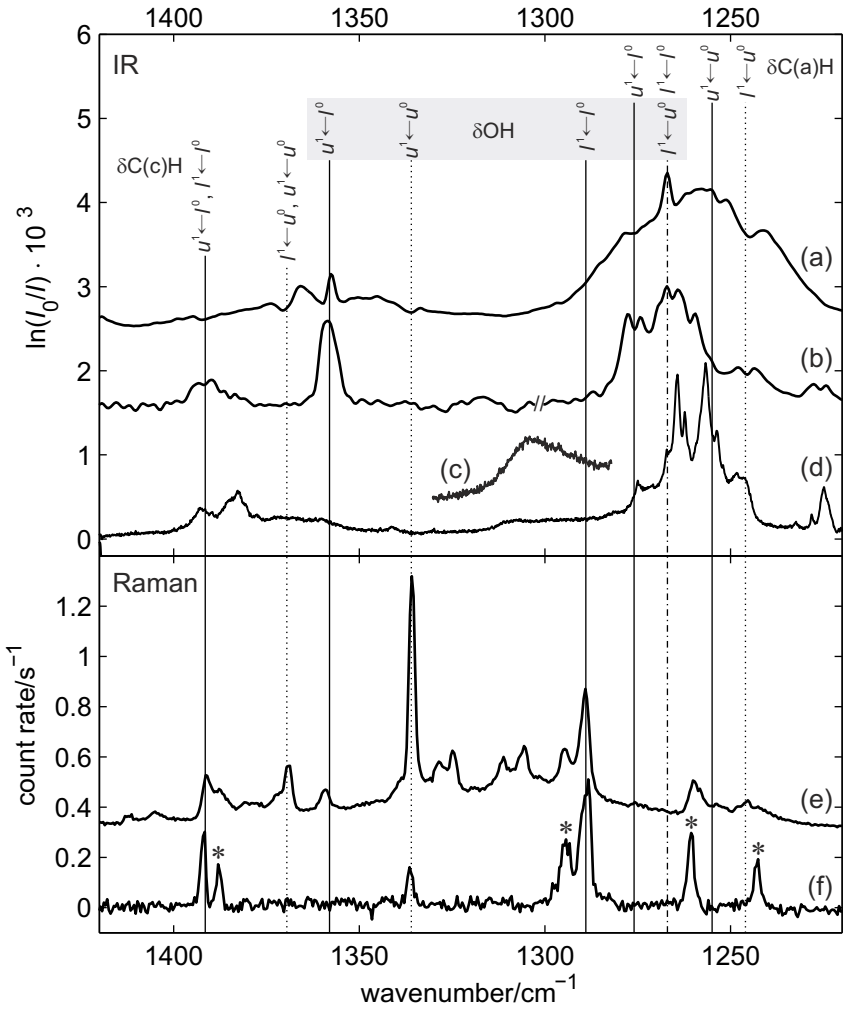

Figure 8. Vibrational spectra of malonaldehyde in the region 1200 – 1400 cm^{-1}; (a) FTIR gas phase spectrum ÷ 30, (b) FTIR jet spectrum, (c) FTIR Ne matrix spectrum ÷ 100, (d) FTIR Ar matrix spectrum ÷ 250, (e) Raman gas phase spectrum ÷ 18, (f) 3 mm Raman Ne jet spectrum; assignment are indicated by solid lines for l^0 transitions, dotted lines for u^0 transitions, and a dash-dotted line for overlapping $\delta\,C_cH$ and $\delta\,OH$ transitions; signals marked with $*$ are assigned to local resonances, see also Ref. [36].

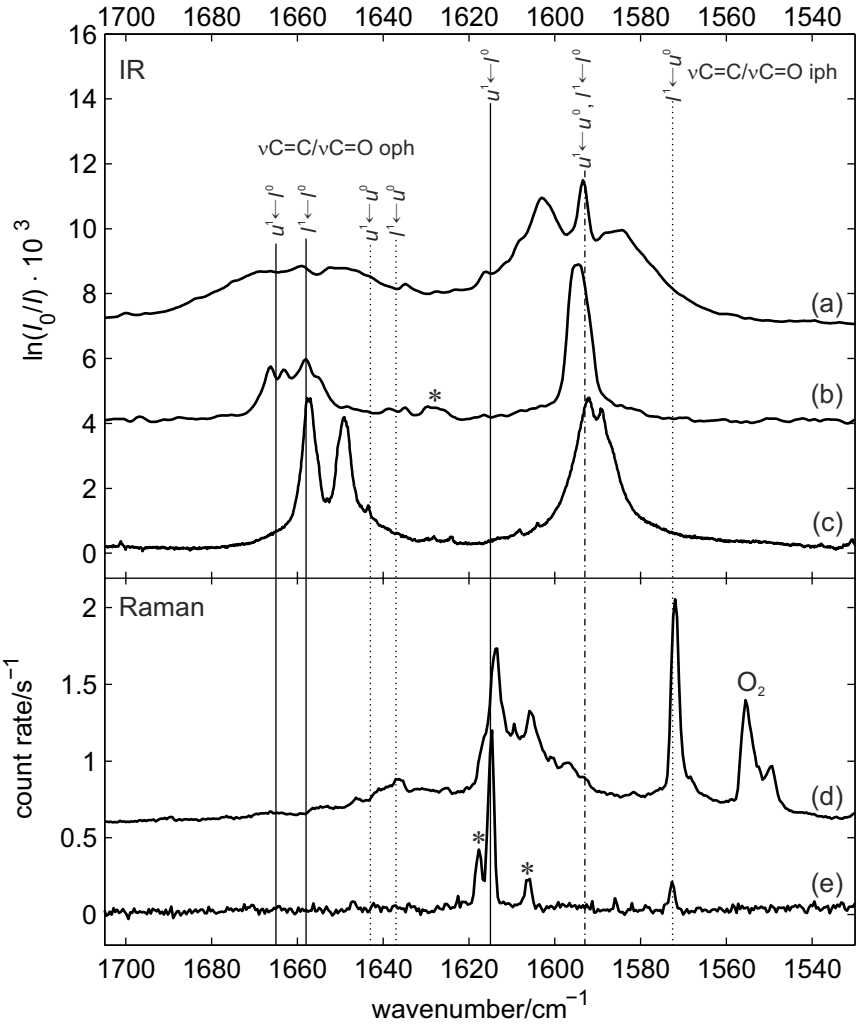

Figure 9. Vibrational spectra of malonaldehyde in the region 1500 – 1700 cm^{-1}; (a) FTIR gas phase spectrum ÷ 30, (b) FTIR jet spectrum, (c) FTIR Ar matrix spectrum ÷ 180, (d) Raman gas phase spectrum ÷ 13, (e) 3 mm Raman Ne jet spectrum; assignment are indicated by solid lines for l^0 transitions, dotted lines for u^0 transitions, and a dash-dotted line for overlapping ν C=C/C=O iph transitions; signals marked with ∗ are assigned to local resonances

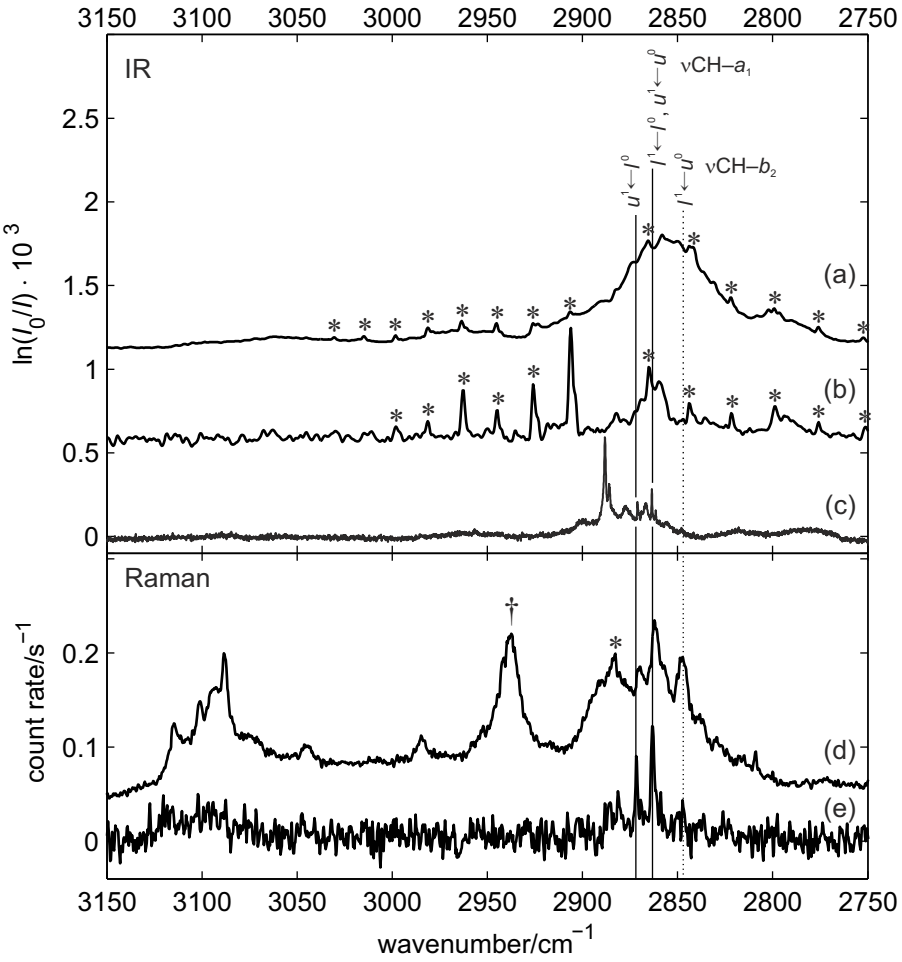

Figure 10. Vibrational spectra of malonaldehyde in the CH stretching region. (a) FTIR gas phase spectrum $\div 10$, (b) FTIR jet spectrum, (c) FTIR Ar matrix spectrum $\div 500$, (d) Raman gas phase spectrum $\div 12$, (e) 1 mm Raman He jet spectrum. HCl signals are marked with $*$, the transition marked with † was not always reproducible. Solid lines indicate l^0 transitions, dotted lines u^0 transitions.

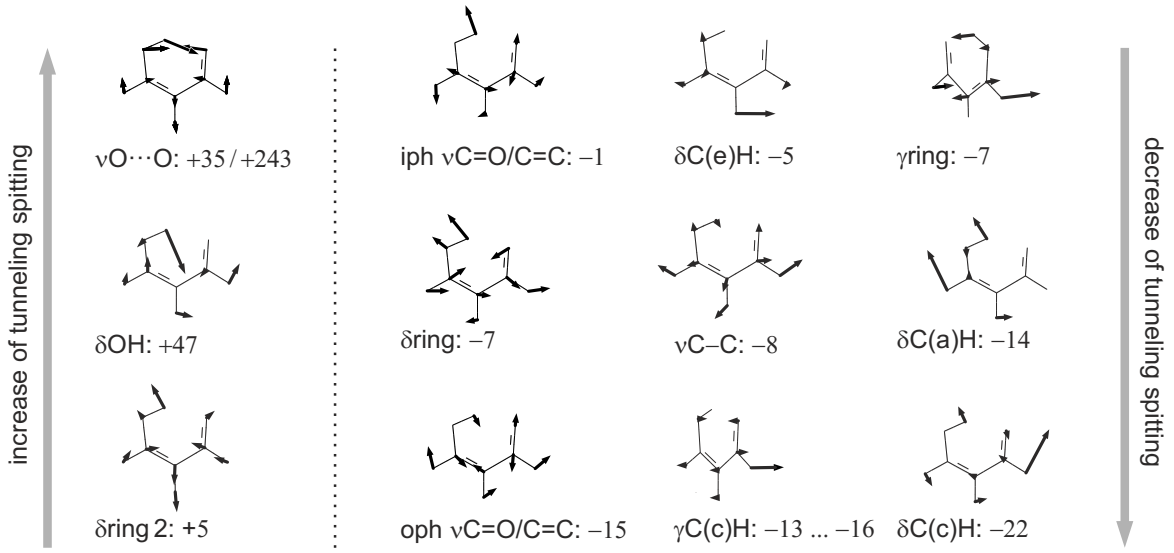

Figure 11. Calculated vibrational normal modes of semi-rigid C_s-symmetric malonaldehyde on the MP2/6-311+G(d) level; the normal modes are ordered according to their impact on the hydrogen transfer. $\Delta\tilde{\nu}^1 - \Delta\tilde{\nu}^0$ values are given in cm^{-1}.

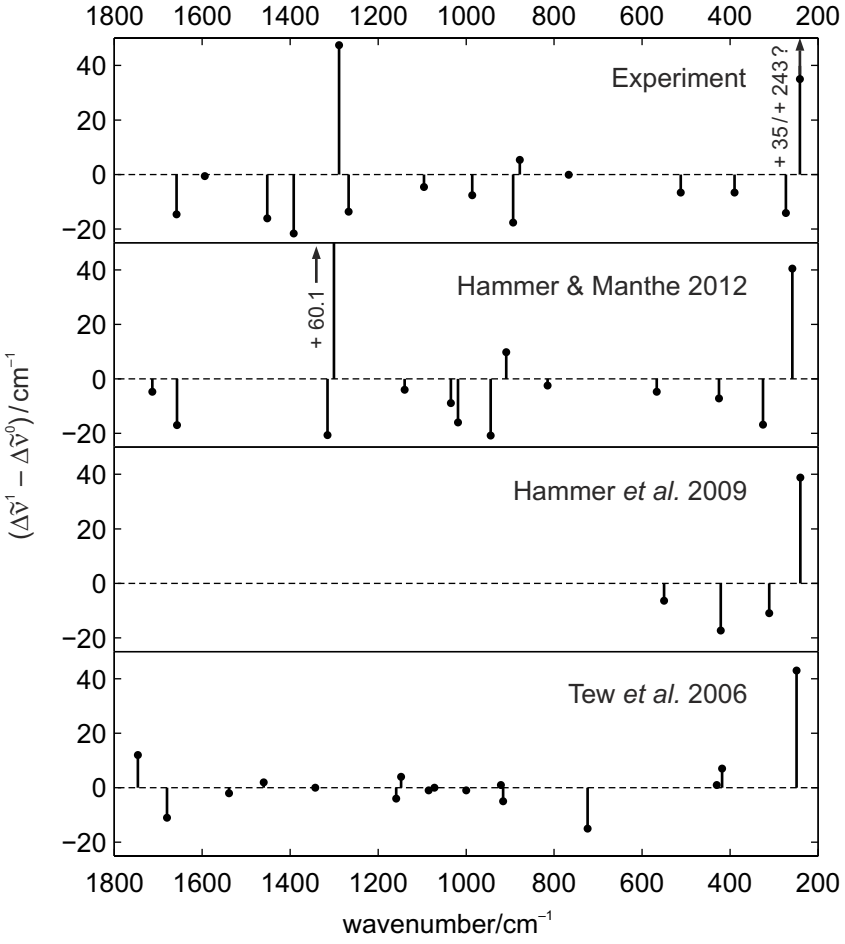

Figure 12. Graphical comparison of the experimental change in tunneling splitting upon fundamental ($v = 1$) excitation ($\Delta\tilde{\nu}^1 - \Delta\tilde{\nu}^0$) [10, 34–36] and recent predictions from Tew *et al.* [31], Hammer *et al.* [32], and Hammer & Manthe [11]; values are calculated relative to the corresponding ground state splitting (see Tab. 3). The position of the sticks corresponds to the $l^1 \leftarrow l^0$ transition.

Tables

Table 1. Calculated vibrational normal modes of semi-rigid C_s-symmetric malonaldehyde: Representations Γ_{C_s}, harmonic wavenumbers $\tilde{\nu}/\mathrm{cm}^{-1}$, IR intensities $I/\mathrm{km\,mol}^{-1}$, Raman activities $A/\mathrm{Å}^4\,\mathrm{u}^{-1}$ and scattering cross sections $\sigma'/10^{36}\,\mathrm{m}^2\,\mathrm{sr}^{-1}$. Published B3LYP/6-311++G** results [52] are also included. γ = out of plane bending, δ = in plane bending, ν = stretching, iph = in phase, oph = out of phase

		MP2/6-311+G*				B3LYP/6-311+G*				B3LYP/6-311++G**			
Assignment[a]	Γ_{C_s}	$\tilde{\nu}$	I	A	σ'	$\tilde{\nu}$	I	A	σ'	$\tilde{\nu}$	I	A	σ'
$\gamma\,\mathrm{C_cH}$ (Q2)	a''	238	8.0	1.7	50	277	4.9	2.3	58	278	4	2.4	60
$\nu\,\mathrm{O\cdots O}$ (Q5)	a'	279	5.0	0.2	5	280	7.6	1.0	25	265	9	0.9	20
γ ring (Q3)	a''	361	3.5	0.9	17	392	2.9	0.5	9	384	4	0.7	10
δ ring (Q4)	a'	500	18.8	4.7	63	511	18.4	4.0	52	508	18	4.0	53
$\gamma\,\mathrm{OH/C_eH}$ iph[b]	a''	705	158	2.0	19	–	–	–	–	–	–	–	–
$\gamma\,\mathrm{OH/C_eH}$ oph[b]	a''	771	0.3	0.1	1	–	–	–	–	–	–	–	–
$\gamma\,\mathrm{C_eH}$[b]	a''	–	–	–	–	785	56	0.3	2.1	770	42	0.1	1
$\gamma\,\mathrm{OH/C_aH}$ (Q6)[b]	a''	–	–	–	–	862	104	1.3	10	882	75	1.5	11
δ ring 2 (Q7)	a'	891	8.9	6.4	46	892	8.5	6.0	42	874	7	6.2	45
$\gamma\,\mathrm{OH/C_aH/C_cH}$ iph	a''	970	28.9	2.5	16	1002	13.4	2.5	15	989	24	1.5	9
ν C–C (Q10)	a'	994	68.1	13.1	82	993	52.1	16.5	103	979	48	17.2	109
$\gamma\,\mathrm{C_aH/C_cH}$ oph	a''	1028	4.9	0.2	1	1036	10.1	0.2	1	1016	13	0.3	2
$\delta\,\mathrm{C_eH}$ (Q11)	a'	1123	20.3	10.5	57	1119	15.2	11.8	64	1094	13	12.6	70
$\delta\,\mathrm{C_aH}$ (Q13/14)	a'	1299	180	3.7	17	1291	179	2.2	10	1262	167	2.1	10
δ OH (Q5/7/18)	a'	1409	44.1	29.4	121	1395	89.9	17	71	1364	101	23.0	98
$\delta\,\mathrm{C_cH}$	a'	1428	39.6	25.3	102	1409	28.6	7.9	32	1372	20	6.3	27
$\delta\,\mathrm{C_aH}/\delta\,\mathrm{C_eH}$	a'	1485	37.5	4.6	18	1479	45.2	3.0	12	1445	49	2.8	11
ν C=O/C=C iph (Q17/18)	a'	1647	304	126	422	1621	314	50.5	173	1587	286	44.6	157
ν C=O/C=C oph (Q16)	a'	1709	204	9.6	31	1704	227	5.4	17	1661	229	5.3	18
$\nu\,\mathrm{C_cH}$	a'	3033	97.6	158	224	2974	111	168	245	2913	105	174	263
$\nu\,\mathrm{C_aH}$	a'	3226	12.2	79.7	102	3175	30.7	97.5	128	3090	112	119	164
$\nu\,\mathrm{C_eH}$	a'	3259	3.0	106	134	3211	7.8	112	144	3150	2	97.6	130
ν OH	a'	3448	114	48	55	3294	139	16	20	3139	125	15.9	21

[a] The transition-state notation from Ref. [11] is given in parenthesis but like the C_{2v} labels of the fundamentals (Tab. 2), it may depend on subtle avoided crossings in the adiabatic picture and on mode mixing.

[b] For some of the out of plane modes the normal coordinates and wavenumbers differ substantially between MP2 and B3LYP calculations and are listed separately.

Table 2. Band positions of the observed (this work) and imported (Refs. [9, 10, 37, 38]) vibrational tunneling-transitions; for labeling see also Fig. 4. The fundamental transitions in Ar matrices are labeled $1 \leftarrow 0$. Signals printed in roman were found in Raman spectra, such printed in italics in IR spectra and signals printed in bold italics were observed with both techniques. Non-rigid representations ($\Gamma_{C_{2v}}$) are proposed as indicated by IR rotational profiles [10], where available. All values are given in cm^{-1}.

		Transition					
Assignment	$\Gamma_{C_{2v}}$	$u^1 \leftarrow l^0$	$l^1 \leftarrow l^0$	$u^1 \leftarrow u^0$	$l^1 \leftarrow u^0$	$1 \leftarrow 0$	$\Delta\tilde{\nu}^1$
malonaldehyde-OH							
$\nu\,\mathrm{O}\cdots\mathrm{O}^c$	a_1	*506*[a], *507*[b]	241	484	*220*[a]	—	265
$\nu\,\mathrm{O}\cdots\mathrm{O}^c$	b_2	241	*184*[a]	*220*[a]	—	—	57
$\gamma\,\mathrm{C_cH}$	—	*282*[a]	273	258	***252***[a]	274[d]	6 ... 9
γ ring	—	405	*390*[a], *391*[b]	*384*[a,b]	—	390[d]	15
δ ring	b_2	527	*512*[a], *513*[b]	*506*[a], *507*[b]	490	510[d], 511[e]	15
δ ring 2	—	—	878	883	—	—	27
ν C–C	a_1	*1000*	986	978	*964*	983	14
$\delta\,\mathrm{C_eH}$	b_2	***1113***	—	—	***1074***	1094	17
$\delta\,\mathrm{C_aH}$	b_2	*1276*	*1267*	*1255*	*1246*	1264	8[f]
δ OH	a_1	*1358*	1289	1336	*1267*	1310	69[f]
$\delta\,\mathrm{C_cH}$	—	***1392***	***1392***	***1370***	***1370***	1383	≈ 0[f]
ν C=O/ν C=C iph	b_2	1615	*1594*	*1594*	1573	1592	21
ν C=O/ν C=C oph	b_2	*1665*	*1658*	—	*1637*	1649	7
$\nu\,\mathrm{CH}{-}a_1$	a_1	—	2863	2863	—	2864	22
$\nu\,\mathrm{CH}{-}b_2$	b_2	2872	—	—	2847	—	3
malonaldehyde-OD							
δ ring 2		—	835	835	—	—	3
ν C–C		—	975	973 ... 974	—	—	1 ... 2
$\delta\,\mathrm{C_eH}/\delta$ OD		1106	—	—	1083	—	20

[a] From Ref. [9]
[b] From Ref. [10]
[c] Alternative tentative assignments
[d] From Ref. [37]
[e] From Ref. [38]
[f] See also Ref. [36]

Table 3. Change of tunneling splitting with respect to the ground state tunneling splitting for fundamental ($v = 1$) excitations $\tilde{\nu}_l$; comparison of experimental results from this work with predictions from Sewell *et al.* [26], Benderskii *et al.* [28], Meyer & Ha [29], Tew *et al.* [31], Hammer *et al.* [32], and Hammer & Manthe [11]; all values given in cm^{-1}

		$(\Delta\tilde{\nu}^1 - \Delta\tilde{\nu}^0)/\mathrm{cm}^{-1}$						
Mode	exp. $\tilde{\nu}_l$	Ref. [26]	Ref. [28]	Ref. [29]	Ref. [31]	Ref. [32]	Ref. [11]	Exp.
$\nu\,\mathrm{O}\cdots\mathrm{O}$	241	+31.6	+15.5	−4.6	+43	+38.8	+40.5	+35/ + 243[a]
$\gamma\,\mathrm{C_cH}$	273	−2.0	−3.7	−7.2	+7	−10.9	−16.8	−16 ... − 13
γ ring	390	+1.8	+1.1	+1.7	+1	−17.3	−7.2	−7
δ ring	512	+2.5	−1.9	+10.4	−15	−6.4	−4.7	−7
δ ring 2	878	+1.2	+7.1	+14.6	+1	—	+9.8	+5
ν C–C	986	+0.5	+10.2	+2.2	0	—	−8.9	−8
$\delta\,\mathrm{C_eH}$	1113	+3.3	+4.0	+13.8	+4	—	−4.0	−5
$\delta\,\mathrm{C_aH}$	1267	+0.4	+19.3	+25.2	0	—	−20.6	−14
δ OH	1358	+5.7	+510.5	+10.7	−2	—	+60.1	+47
$\delta\,\mathrm{C_cH}$	1392	+4.0	+6.3	+6.9	+2	—	—	−22
ν C=O/ν C=C iph	1594	+1.3	−4.7	+3.1	+12	—	−17.0[b]	−1
ν C=O/ν C=C oph	1658	+2.2	+0.8	−2.4	—	—	−4.7[b]	−15
$\nu\,\mathrm{CH}{-}a_1$	2863	0[b]	−0.9[b]	+2.5	−2[b]	—	—	0
$\nu\,\mathrm{CH}{-}b_2$	2872	+0.3[b]	+152.7[b]	+8.0	—	—	—	−19
$\Delta\tilde{\nu}^0/\mathrm{cm}^{-1}$		21.8	21.6	22.0	15	23.3	23.5	21.6[c]

[a] Alternative tentative assignments
[b] Assignment ambiguous
[c] From Ref. [5]

References

[1] M. Quack and M. Stockburger, J. Mol. Spectrosc. **43**, 87 (1972).
[2] S. Albert, P. Lerch, R. Prentner and M. Quack, Angew. Chem. Int. Ed. **52**, 346 (2013).
[3] K.v. Puttkamer, M. Quack and M.A. Suhm, Mol. Phys. **65**, 1025 (1988).
[4] W.F. Rowe, R.W. Duerst and E.B. Wilson, J. Am. Chem. Soc. **98**, 4021 (1976).
[5] T. Baba, T. Tanaka, I. Morino, K.M.T. Yamada and K. Tanaka, J. Chem. Phys. **110**, 4131 (1999).
[6] P. Gilli, V. Bertolasi, V. Ferretti and G. Gilli, J. Am. Chem. Soc. **116**, 909 (1994).
[7] S.L. Baughcum, R.W. Duerst, W.F. Rowe, Z. Smith and E.B. Wilson, J. Am. Chem. Soc. **103**, 6296 (1981).
[8] S.L. Baughcum, Z. Smith, E.B. Wilson and R.W. Duerst, J. Am. Chem. Soc. **106**, 2260 (1984).
[9] Z. Smith, E.B. Wilson and R.W. Duerst, Spectrochim. Acta A **39**, 1117 (1983).
[10] C.J. Seliskar and R.E. Hoffmann, J. Mol. Spectrosc. **96**, 146 (1982).
[11] T. Hammer and U. Manthe, J. Chem. Phys. **136**, 054105 (2012).
[12] T. Carrington and W.H. Miller, J. Chem. Phys. **84**, 4364 (1986).
[13] G.V. Mil'nikov, K. Yagi, T. Taketsugu, H. Nakamura and K. Hirao, J. Chem. Phys. **119**, 10 (2003).
[14] M.D. Coutinho-Neto, A. Viel and U. Manthe, J. Chem. Phys. **121**, 9207 (2004).
[15] A. Viel, M.D. Coutinho-Neto and U. Manthe, J. Chem. Phys. **126**, 024308 (2007).
[16] Y. Wang, B.J. Braams, J.M. Bowman, S. Carter and D.P. Tew, J. Chem. Phys. **128**, 224314 (2008).
[17] A. Hazra, J.H. Skone and S. Hammes-Schiffer, J. Chem. Phys. **130**, 054108 (2009).
[18] T. Hammer and U. Manthe, J. Chem. Phys. **134**, 224305 (2011).
[19] M. Schröder, F. Gatti and H.D. Meyer, J. Chem. Phys. **134** (2011).
[20] Z. Smedarchina, W. Siebrand and A. Fernández-Ramos, J. Chem. Phys. **137**, 224105 (2012).
[21] B. Fehrensen, D. Luckhaus and M. Quack, Z. Phys. Chem. **209**, 1 (1999).
[22] K. Yagi, T. Taketsugu and K. Hirao, J. Chem. Phys. **115**, 10647 (2001).
[23] K. Giese, M. Petković, H. Naundorf and O. Kühn, Phys. Rep. **430**, 211 (2006).
[24] E. Bosch, M. Moreno and J.M. Lluch, Chem. Phys. **159**, 99 (1992).
[25] T.D. Sewell and D.L. Thompson, Chem. Phys. Lett. **193**, 347 (1992).
[26] T.D. Sewell, Y. Guo and D.L. Thompson, J. Chem. Phys. **103**, 8557 (1995).
[27] M. Ben-Nun and T.J. Martínez, J. Phys. Chem. A **103**, 6055 (1999).
[28] V.A. Benderskii, E.V. Vetoshkin, I.S. Irgibaeva and H.P. Trommsdorff, Russ. Chem. Bull., Int. Ed. **50**, 1148 (2001).
[29] R. Meyer and T.K. Ha, Mol. Phys. **101**, 3263 (2003).
[30] D.P. Tew, N.C. Handy and S. Carter, Mol. Phys. **102**, 2217 (2004).
[31] D.P. Tew, N.C. Handy and S. Carter, J. Chem. Phys. **125**, 084313 (2006).
[32] T. Hammer, M.D. Coutinho-Neto, A. Viel and U. Manthe, J. Chem. Phys. **131**, 224109 (2009).
[33] D. Murdock, L.A. Burns and P.H. Vaccaro, Phys. Chem. Chem. Phys. **12**, 8285 (2010).
[34] C. Duan and D. Luckhaus, Chem. Phys. Lett. **391**, 129 (2004).
[35] T.N. Wassermann, D. Luckhaus, S. Coussan and M.A. Suhm, Phys. Chem. Chem. Phys. **8**, 2344 (2006).
[36] N.O.B. Lüttschwager, T.N. Wassermann, S. Coussan and M.A. Suhm, Phys. Chem. Chem. Phys. **12**, 8201 (2010).
[37] D.W. Firth, P.F. Barbara and H.P. Trommsdorff, Chem. Phys. **136**, 349 (1989).
[38] T. Chiavassa, P. Roubin, L. Pizzala, P. Verlaque, A. Allouche and F. Marinelli, J. Phys. Chem. **96**, 10659 (1992).
[39] S.F. Tayyari and F. Milani-Nejad, Spectrochim. Acta A **54**, 255 (1998).
[40] A. Alparone and S. Millefiori, Chem. Phys. **290**, 15 (2003).
[41] V. Barone and C. Adamo, J. Chem. Phys. **105**, 11007 (1996).
[42] S. Sadhukhan, D. Muñoz, C. Adamo and G. Scuseria, Chem. Phys. Lett. **306**, 83 (1999).
[43] C.S. Tautermann, A.F. Voegele, T. Loerting and K.R. Liedl, J. Chem. Phys. **117**, 1967 (2002).
[44] J.T. Hynes, J.P. Klinman, H.H. Limbach and R.L. Schowen, editors, *Hydrogen-Transfer Reactions* (Wiley-VCH, Weinheim, 2006).
[45] Y. Masuda, T. Nakano and M. Sugiyama, J. Phys. Chem. A **116**, 4485 (2012).
[46] D.R. Borst, J.R. Roscioli, D.W. Pratt, G.M. Florio, T.S. Zwier, A. Müller and S. Leutwyler, Chem. Phys. **283**, 341 (2002).
[47] A. Trivella, S. Coussan and T. Chiavassa, Synth. Commun. **38**, 3285 (2008).
[48] Z. Xue and M.A. Suhm, J. Chem. Phys. **131**, 054301 (2009).
[49] T.N. Wassermann, M.A. Suhm, P. Roubin and S. Coussan, J. Mol. Struct. **1025**, 20 (2012).
[50] R.W. Larsen, P. Zielke and M.A. Suhm, J. Chem. Phys. **126** (2007).
[51] A. Trivella, T.N. Wassermann, J.M. Mestdagh, C.M. Tanner, F. Marinelli, P. Roubin and S. Coussan, Phys. Chem. Chem. Phys. **12**, 8300 (2010).
[52] J. Spanget-Larsen, Chem. Phys. **240**, 51 (1999).
[53] M.J. Frisch, G.W. Trucks, H.B. Schlegel, G.E. Scuseria, M.A. Robb, J.R. Cheeseman, J.A. Montgomery, Jr., T. Vreven, K.N. Kudin, J.C. Burant, J.M. Millam, S.S. Iyengar, J. Tomasi, V. Barone, B. Mennucci, M. Cossi, G. Scalmani, N. Rega, G.A. Petersson, H. Nakatsuji, M. Hada, M. Ehara, K. Toyota, R. Fukuda, J. Hasegawa, M. Ishida, T. Nakajima, Y. Honda, O. Kitao, H. Nakai, M. Klene, X. Li, J.E. Knox, H.P. Hratchian, J.B. Cross, C. Adamo, J. Jaramillo, R. Gomperts, R.E. Stratmann, O. Yazyev, A.J. Austin, R. Cammi, C. Pomelli, J.W. Ochterski, P.Y. Ayala, K. Morokuma, G.A. Voth, P. Salvador, J.J. Dannenberg, V.G. Zakrzewski, S. Dapprich, A.D. Daniels, M.C. Strain, O. Farkas, D.K. Malick, A.D. Rabuck, K. Raghavachari, J.B. Foresman, J.V. Ortiz, Q. Cui, A.G. Baboul, S. Clifford, J. Cioslowski, B.B. Stefanov, G. Liu, A. Liashenko, P. Piskorz, I. Komaromi, R.L. Martin, D.J. Fox, T. Keith, M.A. Al-Laham, C.Y. Peng, A. Nanayakkara, M. Challacombe, P.M.W. Gill, B. Johnson, W. Chen, M.W. Wong, C. Gonzalez and J.A. Pople, Gaussian 03 Revision B.04, Gaussian, Inc., Pittsburgh PA, **2003**.
[54] D.A. Long, *The Raman Effect* (John Wiley & Sons, Ltd., Chichester, 2002).
[55] F. Kollipost, R.W. Larsen, A.V. Domanskaya, M. Nörenberg and M.A. Suhm, J. Chem. Phys. **136**,

151101 (2012).
[56] H. Odashima, L.R. Zink and K.M. Evenson, J. Mol. Spectrosc. **194**, 283 (1999).
[57] P. Zielke and M.A. Suhm, Phys. Chem. Chem. Phys. **9**, 4528 (2007).
[58] H.G.M. Edwards, D.A. Greenhalgh, D.A. Long and G. Sherwood, J. Raman Spectrosc. **22**, 467 (1991).
[59] S.F. Tayyari, Z. Moosavi-Tekyeh, M. Zahedi-Tabrizi, H. Eshghi, J.S. Emampour, H. Rahemi and M. Hassanpour, J. Mol. Struct. **782**, 191 (2006).
[60] J. Spanget-Larsen, B.K.V. Hansen and P.E. Hansen, Chem. Phys. **389**, 107 (2011).
[61] N. Došlić and O. Kühn, Z. Phys. Chem. **217**, 1507 (2003).
[62] P. Hamm and G. Stock, Phys. Rev. Lett. **109**, 173201 (2012).
[63] R.R. Lozada-Garcia, J. Ceponkus, M. Chevalier, W. Chin, J.M. Mestdagh and C. Crépin, Angew. Chem. Int. Ed. **51**, 6947 (2012).
[64] V.E. Bondybey, R.C. Haddon and J.H. English, J. Chem. Phys. **80**, 5432 (1984).